Manuscript prepared for Hydrol. Earth Syst. Sci. Discuss.
with version 2014/05/30 6.91 Copernicus papers of the LaTeX class copernicus.cls.
Date: 24 November 2014

Authors' response on "Thermal damping and retardation in karst conduits" *by* A. J. Luhmann et al.

Andrew J. Luhmann[1], Matthew D. Covington[2], Joseph M. Myre[2], Matija Perne[2,3], Sidney W. Jones[4], E. Calvin Alexander, Jr.[1], and Martin O. Saar[1,5]

[1]University of Minnesota, Department of Earth Sciences, 310 Pillsbury Dr. SE, Minneapolis, Minnesota, 55455, USA
[2]University of Arkansas, Department of Geosciences, 216 Ozark Hall, Fayetteville, Arkansas, 72701, USA
[3]Jožef Stefan Institute, Department of Systems and Control, Jamova Cesta 39, Ljubljana, Slovenia
[4]527 Karrow St., Maryville, Tennessee, 37803, USA
[5]ETH-Zürich, Geothermal Energy and Geofluids Group, Department of Earth Sciences, Zürich, CH

Correspondence to: A. J. Luhmann
(luhm0031@umn.edu)

Dear Jesus Carrera,

Below we include our responses and manuscript changes (in plain text) to address your comments (in bold text). We also include our responses (in plain text) to each comment of the Referees (in bold text) that were originally published as Interactive Comments. Finally, we include text in italics to indicate how/where the manuscript was changed in response to comments from the Referees. Page and line numbers refer to the marked-up manuscript version.

Thank you for your comments and handling of our manuscript.

Sincerely,

Andrew Luhmann

Editor Initial Decision: Publish subject to minor revisions (Editor review) (05 Nov 2014) by Jesús Carrera

Comments to the Author: I feel that the reviewers comments are quite positive, specific and relatively easy to address (but see below).I am convinced you will have no problems in accommodating them. In any case, I will wait for your final version and response to comments to decide whether or not to request another round of revisions prior to final publication in HESS.

I'd suggest to emphasize the following issues in your response:

1)variable velocity. All reviewers point it out, and it is relevant in practice. While I understand that it is beyond an analytical solution, all readers would like to know the effect of this simplification. Since you are using comsol for numerical simulations, I'd suggest to expand somewhat the comparison of your analytical solution with numerical simulations. In this case, I'd suggest working with "pore volume" equivalent time(i.e., integral from 0 to t of Q(t)dt divided by Average Q).

We have rerun the constant velocity simlations in Sect. 7.3.2 so that both the constant velocity and variable velocity simulations in each simulation set have the same flow-through time. This changes the results relatively little, but it facilitates a better comparison with equal flow-through times. It would be difficult (perhaps impossible) to generalize the effect of variable velocity with additional simulations. Furthermore, the way we ran the variable velocity simulations in Sect. 7.3.2 is not unique, and there are an infinite number of possibilites. That said, the analytical solutions can be used to know the effect of the constant velocity simplification, and we now include an example case that uses the analytical solutions to provide general bounds of uncertainty when velocity is variable. We also note that while there may be too much uncertainty with the constant velocity assumption in some field scenarios, our multitracer experiments at Freiheit Spring provided useful results even with variations in velocity. The expanded discussion of the constant velocity simplification is found on pages 32-33 (lines 729-748).

2) The issue of inflow (not so much outflows, I believe) mentioned by the reviewers deserves more attention than given in your published reply. As a potential user, I'd like to know how to address the "cooling effect" of cool water inflow into the conduit on a hot water pulse input.

Inflow water will change the temperature of the water in the conduit if the two temperatures are different. However, this thermal modification is due to mixing of two water sources with different temperatures or dilution of the input rather than damping that occurs due to heat exchange between water and rock. The influence of dilution on the transmission factor can be approximated using a simple mixing model, so long as the signal is not severly damped. In this case, the peak input temperature is first reduced to account for the dilution before the thermal transmission factor is calculated.

We added new text on pages 33-34 (lines 749-774) that further discusses the effects of hydraulic exchange between the conduit and matrix, using data from the multitracer experiment in Luhmann et al. (2012) to illustrate our discussion.

3)I'd also consider relevant the energy balance issue brought up by Ron Green

In response to the energy balance issue brought up by Ron Green, we have added the temperature of the water input from the second multitracer experiment to the text, a summary of the energy budget from the multitracer experiment described in Luhmann et al. (2012), and transmission and heat recovery calculations from the second experiment. These components with additional discussion more fully explores the energy balance and can be found on pages 24-27.

4) I would add that from a practical point of view, you should be able to provide some suggestion on the conditions under which the test is worth trying (e.g., if the conduit is very long, I'd need a very long heat pulse to be able to observe anything in the output), Can you provide some specific easy-to-follow rule?.

The ratio of conduit length to the thermal length scale given in Eq. (23) can be used to determine if a thermal tracer test is likely to produce a thermal perturbation in the output. When this ratio is $\lesssim 1$, a test should produce a water temperature change at the outlet. When this ratio is $\gg 1$, input thermal pulses will be completely damped. When conducted, thermal tracer tests will confirm or illustrate errors in parameter estimates, and thus, will always provide useful results.

This component has been added to page 36 (lines 829-840).

The paper is good! Go ahead!

Below you will find our responses (in plain text) to the comments from Anonymous Referee #1 (in bold text). We thank Anonymous Referee #1 for his/her time and effort in helping us to improve our manuscript.

The authors present analytical and numerical solutions for relating conduit geometry with thermal damping and retardation. The manuscript is overall well written and the topic interesting. Moreover, the findings are of interest of the scientific community and may be useful to give some light in inferring karst conduit properties. I have not reviewed the mathematical development for analytical solutions. It seems to be correct but I leave this task to another referee.

Although I consider that the manuscript is acceptable for publication at Hess in its current format, I propose some minor issues that, in my opinion, could improve this manuscript: - Section 5 page 9602; Hydraulic boundary conditions are not clear. The authors impose velocity just at the conduit or fracture inlet? Is there flow across the matrix? The authors say that the calculation of f does not affect to the results. Is the model insensitive to this parameter or is it a consequence of the imposed boundary conditions? What if you impose head instead of velocity?

We will clarify our hydraulic boundary conditions. Velocity is imposed along the entire conduit. As most simulations model full pipe flow, there are no spatial velocity gradients. The model does not incorporate flow across the matrix, but we do briefly discuss the effects of dilution from more diffuse flow paths on thermal damping and retardation.

The value of f does affect the results, and the model is sensitive to this parameter. However, simulation results do not depend on whether the von Kármán Equation or the Colebrook-White Equation is used to calculate f.

There is no difference in the model if we impose head instead of velocity. Each velocity used in the simulations is equivalent to a specific hydraulic head, given the particular properties of the flow path. In karst conduits with full pipe flow, the Darcy-Weisbach equation relates head to velocity.

The hydraulic conditions have been clarified with the new conceptual model section on page 5 (lines 96-104), and the effects of flow across the matrix are more fully developed on pages 33-34 (lines 749-774).

The authors explain the number of elements within the grid but it would be more useful an explanation of the model sensitivity to this grid (it seem they have some numerical dispersion that could be produced because of a grid effect). What about the time stepping? –

We will add a brief discussion that clarifies that neither the grid nor the time stepping affected the modeled results. We increased the number of elements to increase the grid resolution and decreased the relative and absolute tolerances (which control time-stepping in COMSOL) to decrease the time stepping for some simulations that appear to be affected by numerical dispersion. However, neither of these changes provided different results.

We have stated that several example cases were run at higher spatial and temporal resolution and produced the same results on page 15 (lines 289-290).

Section 6.3.2, page 9610; Regarding the variable velocity setting I miss a figure showing the fitting between analytical solutions and numerical simulations and an explanation about why the authors chose that range of velocities. As it is the most interesting case, I would pay more attention to this topic.

In the variable flow velocity section, we chose a range in velocity that mimics flow in a natural conduit, although this choice is certainly not unique. Furthermore, we chose to vary velocity using a Gaussian function, which is only one of many possible approximations of natural pulses. It would be difficult if not impossible to develop a general understanding of the effect of variable velocity on thermal damping and retardation relationships.

We have added a statement about our choice of velcity variation on page 32 (lines 729-731).

The modeling work seems to be correct, crossing a wide range of different assumptions. I have noticed some limitations of the model while reading the manuscript, however, they are well discussed on section 8.2 so nothing to say. - Section 7, page 9616;

As for the field study, the authors chose as a section title "An example field study to test the theory". I do not see the testing, I can see a good application to estimate the geometry of conduits applying their solutions but I cannot see how the authors check that the estimation of conduit diameter is correct. Explain better or change the title to something like "Theory application to a field study". The authors claim within the abstract too that they have confirmed their relationships with a tracer experiment. They should change that affirmation if they do not explain better within section 7.

We will modify the text so that it is clear that we are testing a portion of the theory. We conducted two tracer studies at the same site three days apart. The only variable that changed significantly from one study to the next was recharge duration. Because of this, we derive Eq. (53) and use the recharge durations from both studies as well as the thermal retardation during the first study to predict the thermal retardation during both pulses of the second study. There is good agreement between this prediction and the actual retardation values from the second study. In this way, we tested a portion of the theory. Furthermore, we will add some discussion about an excavation at the field site that supports our estimates of hydraulic diameter based on the damping and retardation relationships.

We have revised the Abstract (line 16) and section heading of Sect. 8 (line 508) to make it clear that we tested components of the theory. Furthermore, we added a paragraph at the end of Sect. 8 (pages 27-28, lines 604-617) that discusses observations from excavations at the field site that are in agreement with predictions based on damping and retardation of thermal signals.

Some technical corrections: - Page 9616, line 3: explict would be explicit - Page 9612, line 10: simlations would be simulations –

We will correct these typos.

These typos have been corrected.

Table 6: when the authors explain what Θ means they say advection and conduction time ratio. I would say conduction and advection time ratio, it may lead to errors while reading.

We will correct this definition.

This definition has been corrected.

Below you will find our responses (in plain text) to the comments from Referee R. T. Green (in bold text). We thank R. T. Green for his time and effort in helping us to improve our manuscript.

The subject paper builds on a sequence of recent papers that explore heat flow through karst media. The mathematical development builds on work by Hauns et al. (2001) and Covington et al. (2009, 2011, 2012) using data from a field-scale experiment described in Luhmann et al. (2012). Much of the mathematical model in the subject paper is introduced in the Hauns et al. (2001) paper and further developed in the Covington et al. (2009, 2011, 2012) papers and the dissertation by Luhmann (2011). The subject paper clearly describes the governing equations. The authors then discuss at length analytical and numerical solutions to the advection-dispersion equation to evaluate thermal damping and retardation for cylindrical and planar geometries chosen for representing karst solution features.

The authors solve the equations for a sinusoidal signal chosen to represent the pulse of heated and tagged water injected into a sinkhole during the field-scale experiment. The authors make simplifying assumptions when solving these equations. Although solving the equations without making these assumptions would be challenging, there is some question whether these assumptions are appropriate. Of concern is the assumption of constant velocity. In particular, the temperature of the water input into the cylindrical or planar conduit is represented as sinusoidal but flow is constant (Eq. 34).

Derivations of relatively simple analytical solutions require simplifications, one of which is the constant velocity assumption. It is possible that this assumption will introduce too much uncertainty and limit the applicability of the damping and retardation analytical solutions in some field scenarios. However, a conduit fed by a sinking stream will have periods of relatively constant velocity between recharge events even while there are diurnal variations in water temperature. In this case, the analytical solutions are directly applicable to field settings, at least in terms of the constant velocity assumption. We noted that interpretation of damping and retardation data is most easily accomplished in these systems when flow-through time is relatively constant. Still, it is possible that the analytical solutions provide useful results, even when the assumptions are not valid. Velocity was not constant during our field experiments at Freiheit Spring. In Luhmann et al. (2012), the best fitting numerical simulation of the thermal pulse from the first experiment incorporated a flow path with a hydraulic diameter of 7 cm in planar coordinates, and the numerical simulations incorporated the variations in velocity. If we assume that velocity was constant and use the average flow-through time in the conduit, then the average of the two estimates of hydraulic diameter using both the damping and retardation data is 6.5 cm.

The field-scale experiment was described in a separate paper by Luhmann et al. (2012) which described how a volume of 13,000 L of water was heated and spiked with tracers, then injected into a sinkhole in 3-1/2 minutes. The temperature of the injected water was not reported, but groundwater temperatures at the spring discharge located at a distance of 95 m increased by a maximum of about 2.5°C. This input is consistent with the assumption of sinusoidal temperature at the upstream boundary, but violates the assumption of constant velocity in Eq. (34) thereby raising a question whether the numerical solution is valid. The solution may be valid if velocity is assumed constant during the injection of the pulse, however this assumption is not noted. Given the description of discharge in Fig 3a in Luhmann et al. (2012), however, this assumption does not appear to be supported.

The manuscript includes data from two field-scale experiments. The first experiment was described in Luhmann et al. (2012), and the publication includes the temperature of the injected water (24.1°C). The second experiment was conducted at the same site three days later, and data from this experiment is described for the first time in this manuscript. The temperature of the injected water was included in Fig. 6 (21.5°C), but we will also include this temperature in the text to prevent any confusion. In Luhmann et al. (2012), we concluded that the pressure pulse, which indicated full pipe flow conditions, suggests that the flow path's cross-sectional area was likely constant. Therefore, the variation in discharge corresponds to a variation in velocity during both field experiments. We acknowledge that variations in velocity will cause uncertainty in Eqs. (36), (37), and (38). However, even with this uncertainty, we note that estimates of hydraulic diameter using Eqs. (36) and (38) are comparable to and bound the estimate in Luhmann et al. (2012) from heat transport simulations that include variations in velocity.

The 21.5° C pool water temperature has been added to the text on page 25 (line 528) and the figure caption of Fig. 6.

When discussing the results, the authors introduce time-averaged or reference flow velocity (Eq. 37) when establishing the terms for agreement in thermal transmission between planar and cylindrical heat transport and determine a correction factor is needed. The correction term is dependent on the time-average flow velocity. Later on, the authors comment that scatter in the cylindrical solution at relatively slow velocities may be due to numerical scatter. This correction factor in the solution for planar flow may be needed to overcome the assumption of constant velocity.

It is unlikely that there is a simple correction factor that would provide agreement between constant and variable velocity scenarios. Even if there were, such a correction factor would be different from the correction factor given in Eq. (37).

The authors discuss the implications of assuming constant velocity in Section 6.3.2 and evaluate the impact of this assumption by comparing numerical simulations with and without constant velocity. The comparisons suggest that thermal retardation is affected by a maximum of 30 % occurred when the ratio of recharge duration to flow-through time is decreased (Table 3). In other words, the discrepancy is increased for systems in which the duration of recharge is small relative to the velocity and the spatial distance between the locations of recharge and discharge (i.e., flow-through time).

The relationship in retardation variability between constant and variable velocity simulations is complex. Variability in thermal retardation between constant and variable velocity simulations increased for most of the sets as the ratio of recharge duration to flow-through time decreased. However, the set that had the lowest recharge duration to flow-through time ratio had the second lowest retardation variability between constant and variable velocity simulations.

We have noted the difficulty of generalizing the variable velocity effect on page 32 (lines 731-732).

The authors further elaborate on the qualifying assumptions in Sections 8.1 and 8.2 (Limitations). They note that velocity only occurs twice in the final solution, Eq. (36) and (38), and that it is included as the flow-through time (L/V). The Limitations section (8.1) provides minimal discussion on the ramifications when assuming constant velocity.

We will add some additional discussion on the limitations of the constant velocity assumption, noting that this assumption may introduce too much uncertainty in some field settings.

Additional discussion of the constant velocity assumption has been included on pages 32-33 (lines 729-748).

It would be informative for the authors to expand on the assumption of constant velocity. It is obvious that the severity of the assumption of constant velocity is dependent on spatial scale, introducing more uncertainty and inaccuracy when the flow-through time becomes relatively large. Providing a graph of how uncertainty or inaccuracy increases with flow-through time would be instructive. Partial data for such a graph is already provided in Table 3. Additional data could be provided with limited additional comparisons similar to those used to create the data in Table 3. Such a graph would provide readers a better sense on when the assumption of constant velocity relative to travel time inherent in the assessment become too large as to be unacceptable.

Of the five simulation sets in Table 3, the one with the largest flow-through time had the second lowest variability in thermal retardation. Therefore, the constant velocity assumption does not necessarily introduce more uncertainty and inaccuracy when the flow-through time becomes relatively large. Because of this, it is difficult to generalize when the constant velocity assumption introduces large errors.

We have added calculations using the analytical solutions that provide some bounds on uncertainty due to variations in velocity on pages 32-33 (lines 731-744).

Would it be possible to report the temperature of the water that is input? This could possibly allow evaluation of the energy budget. It would be necessary to assume the thermal properties of the host rock and make assumptions on the constitutive relations of heat transfer, but insight on thermal damping and retardation could be gained by such an assessment.

We will add the temperature of the water input from the second field experiment (21.5°C) to the text, although it was already included in Fig. 6. The temperature of the input from the first field experiment (24.1°C) was included in Luhmann et al. (2012). We have already included the thermal retardation data from both field experiments in the current manuscript. Our calculation of damping from the first field experiment is detailed in Luhmann et al. (2012), but we do not calculate damping from either pulse of the second field experiment because no samples were analyzed for chloride and there was more thermal variability in the spring water before the second field experiment, both of which increase uncertainty in a damping calculation.

An evaluation of the energy budget from the first study was provided in Luhmann et al. (2012), where we calculated a lower heat recovery than either dye or salt recovery over the first two hours of the experiment. This lower heat recovery occurred because of the damping of the thermal signal, where some of the heat was transferred into the rock surrounding the flow path. We also noted that heat from the heated rock was later transferred to subsequent water that flowed along the flow path, since water temperature at the spring remained higher than its background after experiment water no longer reached the spring. There is more uncertainty in the evaluation of the energy budget from the second experiment because of the reasons noted above which introduce uncertainty in the damping calculation.

The 21.5° C pool water temperature has been added to the text on page 25 (line 528) and the figure caption of Fig. 6, and we briefly summarize the energy budget evaluation from the earlier study reported in Luhmann et al. (2012) on page 24 (lines 514-521). We have also added transmission and heat recovery calculations from the second experiment and additional discussion to evaluate the energy budget on pages 26-27 (lines 577-589).

In summary, the paper is well organized and well written. It relies heavily on the series of papers leading up to it (Covington et al., 2009, 2011, 2012; Luhmann, 2011; Luhmann et al., 2012). This is not to imply that the paper does not make a substantive contribution, it does, but by relying on this proven path, a lot of the developmental work regarding the theory was well established. I would ask that the authors examine the concern that velocity may not be assumed to be constant and to consider exploring the energy balance. Evaluating the energy balance could provide insights on energy transport and thermal damping. This latter suggestion might be best left to a subsequent publication.

Please see our responses above regarding the constant velocity assumption and the energy balance.

Below you will find our responses (in plain text) to the comments from Anonymous Referee #3 (in bold text). We thank Anonymous Referee #3 for his/her time and effort in helping us to improve our manuscript.

The authors present a novel methodology to characterize karst conduit systems. Based on analytical and numerical models they investigate the effect of various system properties on transmission and retardation of heat signals. Finally, the analytical solution allows to characterize the conduits hydraulic diameter based on measured transmission and retardation of heat signals. A conducted field experiment is used to demonstrate the approach. The paper is well structured and written, extensive, and comprehensible.

What I missed was a proper explanation of the underlying conceptual model. After the introduction, the paper starts immediately with a description of the mathematical model. I'd suggest to add some description of the conceptual model prior to the mathematical model, i.e. which processes are considered and which are neglected (maybe Fig. 1 can be modified). In doing so, the authors could help readers to understand some of the limitations of the approach (which are, however, well explained in the latter part of the manuscript, p 9617, line 17ff).

We will add an explanation of the underlying conceptual model.

We added a new section (Sect. 2) on page 5 (lines 92-106) that describes the conceptual model.

One significant conceptual limitation is the missing consideration of variable conduit hydraulics that interact with the matrix. From my understanding, the models assume constant (steady-state) hydraulics for most of the setups (except what is described in section 6.3.2) and there is no interaction between conduit and matrix hydraulics (hydraulically isolated conduit). In consequence, the models cannot consider processes related to varying hydraulics like storage, or water transfer with the surrounding matrix. I assume that for some real situations these processes can be significant: for example an event induced increase of discharge will result in an increase of conduit hydraulic heads; subsequently, this head change potentially affects water transfer with the matrix continuum (matrix storage) or with other fractures or cavities (conduit storage). The authors touch this topic (discussion of water addition along the conduit; p9619, line 19ff). I suggest to discuss this limitation more in detail (in section 8.2 and / or related to the conceptual model). Maybe the paper from Birk et al. (2006) is helpful because the numerical model used there overcome some of the limitations.

We will discuss the limitation of neglecting matrix exchange in more detail. Hydraulic interaction between the conduit and matrix could cause variations in the hydraulic diameter and/or flow velocity as well as affect heat flux in the matrix. Still, we have been able to re-produce output temperature signals relatively well at three sites without considering matrix exchange (Covington et al., 2011; Luhmann et al., 2012).

Additional discussion is now included on pages 33-34 (lines 749-774) that more fully describes the effects of hydraulic exchange between the conduit and matrix.

Specific comments:

• The authors use two different model setups with a cylindrical conduit and a fracture (see Fig. 1). For me the reason in doing so is not always comprehensible. The fracture model setup is introduced at page 9594 line 20. Maybe the authors can add some explanation why this setup is considered (I found something on p9611 line 11).

We will add more discussion. One reason we use the fracture model setup is because it is simpler than a cylindrical model setup. Heat exchange in a cylindrical conduit can be approximated by heat exchange in planar coordinates in many cases (Covington et al. (2012). Furthermore, flow in karst aquifers occurs not only through cylindrical conduits, but also through fractures with a planar geometry. In Luhmann et al. (2012), planar simulations reproduced the thermal signal much better than cylindrical simulations, suggesting that a planar geometry assumption for the particular flow path is much better than a cylindrical one. The planar geometry is also in agreement with field observations.

Further explanation is now included on page 7 (lines 136 and 139-141).

• Can Equation 13 be moved to section 3.1 (similar to Equation 24, which is in 3.2)?

We will make this change.

Eq. (13) is now in Sect. 4.1 (which used to be Sect. 3.1).

• Can Equation 12 be generalized (for planar and cylindrical case)?

We will make Eq. (12) more general.

Eq. (12) is now more general.

- **Some numerical models have different conduit lengths but the discretization remains at 1000 discretized elements (page 9602, line 10 ff). Why is the discretization along x not kept constant (i.e. same element size)?**

The COMSOL model used is dimensionless, so each element is always the same fraction of the entire conduit length (i.e., 1/1000). However, increasing the number of elements for a relatively long conduit does not affect simulation results.

We now note that several example cases were run at higher spatial resolution and produced the same results on page 15 (lines 289-290).

- **At p9619, line 19ff water addition along the conduit is discussed. What about losing water (flow from conduit to matrix or to some other storage)?**

Flow from the conduit to the matrix will affect heat flux in the matrix. The changed heat flux in the matrix would only have a small, indirect influence on the temperature in the conduit, while flow from the matrix to the conduit would have a direct and significant effect on the conduit temperature.

This is now discussed on page 33 (lines 750-752).

- **In Figure 2 the numerical models for small transmission differ from analytical results (first elements along the x-axis until F $\sim$ 0.05). Is there an explanation why corresponding numerical results seems to be zero?**

All of these cases include relatively small diameters. Smaller cylindrical conduits have larger conduit wall surface area to water volume ratios and a greater ratio of thermal penetration depth to conduit radius, which causes additional heat exchange when compared to equivalent planar systems. In this case, the simple correction factor in the cylindrical analytical solution overestimates the amount of transmission that would occur. However, the differences here are relatively minor and no different than the differences in other regions of Fig. 2.

• **Some further data for the field experiment would be helpful to understand the situation without reading Luhmann et al. 2012 (e.g. distance between sinkhole and spring, some information about the sinkhole like distance to the conduit). What about heat recovery?**

We will add some additional data.

We have added further data for the field experiment as well as the heat recoveries from the Luhmann et al. (2012) study and the double pulse study to Sect. 8.

• **If possible, please discuss the results of the field study (D_{H}) little more. The obtained hydraulic diameter D_{H} seems very small. Luhmann et al. (2012) helps to understand these results but some short interpretation can be given here too.**

We will further discuss the results of the field study.

The results of the field study are further discussed at the end of Sect. 8 (lines 604-617).

Suggested technical corrections

• **Equation 15: explanation for X, Y (and R in equation 25)**

The functions $X(x)$, $Y(y)$, and $T_t'(t)$ in Eq. (15) and $X(x)$, $R(r)$, and $T_t'(t)$ in Eq. (25) are factors giving $T_{\mathrm{r}}'(x,y,t)$ and $T_{\mathrm{r}}'(x,r,t)$, respectively, when multiplied.

• **Page 9611 line 9: add “m” behind DH = 1**

We will add the unit.

This has been corrected.

• **Table 3, first data line: delete comma at L/V value**

We will correct this.

This has been corrected.

Manuscript prepared for Hydrol. Earth Syst. Sci. Discuss.
with version 2014/05/30 6.91 Copernicus papers of the LaTeX class copernicus.cls.
Date: 24 November 2014

Thermal damping and retardation in karst conduits

A. J. Luhmann[1], M. D. Covington[2], J. M. Myre[2], M. Perne[2,3], S. W. Jones[4], E. C. Alexander Jr.[1], and M. O. Saar[1,5]

[1]University of Minnesota, Department of Earth Sciences, 310 Pillsbury Dr. SE, Minneapolis, Minnesota, 55455, USA
[2]University of Arkansas, Department of Geosciences, 216 Ozark Hall, Fayetteville, Arkansas, 72701, USA
[3]Jožef Stefan Institute, Department of Systems and Control, Jamova Cesta 39, Ljubljana, Slovenia
[4]527 Karrow St., Maryville, Tennessee, 37803, USA
[5]ETH-Zürich, Geothermal Energy and Geofluids Group, Department of Earth Sciences, Zürich, Switzerland

Correspondence to: A. J. Luhmann (luhm0031@umn.edu)

Abstract

Water temperature is a non-conservative tracer in the environment. Variations in recharge temperature are damped and retarded as water moves through an aquifer due to heat exchange between water and rock. However, within karst aquifers, seasonal and short-term fluctuations in recharge temperature are often transmitted over long distances before they are fully damped. Using analytical solutions and numerical simulations, we develop relationships that describe the effect of flow path properties, flow-through time, recharge characteristics, and water and rock physical properties on the damping and retardation of thermal peaks/troughs in karst conduits. Using these relationships, one can estimate the thermal retardation and damping that would occur under given conditions with a given conduit geometry. Ultimately, these relationships can be used with thermal damping and retardation field data to estimate parameters such as conduit diameter. We also examine sets of numerical experiments where we relax some of the assumptions used to develop these relationships, testing the effects of variable diameter, variable velocity, open channels, and recharge shape on thermal damping and retardation to provide some constraints on uncertainty. Finally, we discuss a ~~tracer~~ multitracer experiment that provides some field confirmation of our relationships. High temporal resolution water temperature data are required to obtain sufficient constraints on the magnitude and timing of thermal peaks and troughs in order to take full advantage of water temperature as a tracer.

1 Introduction

Much of the flow and transport through karst aquifers occurs via conduits (Atkinson, 1977b; Worthington, 1999; Worthington et al., 2000). These preferential flow paths occur in all karst aquifers, but most are poorly characterized or unknown. Hydrogeological investigations of karst aquifers frequently employ hydrographs, chemographs, and thermographs collected from boreholes and springs. Ideally, these data could be used to provide flow path information, and this characterization would facilitate models that are more capable of predicting flow and transport through these systems.

Hydrographs have been analyzed for more than a century (Boussinesq, 1903, 1904; Maillet, 1905) to characterize flow recession, determine aquifer characteristics, or predict discharge with time (e.g., see summaries in Hall, 1968; Tallaksen, 1995; Jeannin and Sauter, 1998; Dewandel et al., 2003; Ford and Williams, 2007). However, hydrographs provide minimal information about conduit geometry (Covington et al., 2009), and interpretations of karst aquifer structure based on hydrograph analysis are problematic because of the relatively strong control of rainfall frequency on hydrograph shape (Jeannin and Sauter, 1998). Variations in specific conductance often occur with changes in localized recharge ~~(Jakucs, 1959; Newson, 1971; Ternan, 1972; Atkinson, 1977a; Atkinson, 1977b; Worthingto~~ While chemical modification of electrical conductivity signals due to dissolving calcite could theoretically be used to constrain the geometry of flow paths with hydraulic diameters on the mm- to cm-scale, electrical conductivity provides little information about conduits with diameters on the meter-scale and larger, because these larger flow paths produce negligible chemical modification of localized recharge from dissolution (Covington et al., 2012).

Conduits facilitate fast flow-through times and may enable thermal perturbations to reach a spring (e.g., Benderitter et al., 1993; Bundschuh, 1997; Martin and Dean, 1999; Screaton et al., 2004; Luhmann et al., 2011). These perturbations are modified as water flows through the system, and the modification is sensitive to conduit geometry (Renner, 1996; Liedl et al., 1998; Liedl and Sauter, 1998). The modification occurs because of the heat exchange between water and rock, causing both damping (i.e., decrease in signal amplitude) and retardation (i.e., time lag of the signal) of recharge (Luhmann et al., 2012). Studies have also demonstrated thermal damping and retardation in porous media (e.g., Molson et al., 1992; Palmer et al., 1992; Markle and Schincariol, 2007) and fractures (e.g., Molson et al., 2007). The non-conservative nature of water temperature, even within fairly large conduits, facilitates estimates of conduit size via an analysis of input and output thermographs (Covington et al., 2011; Covington et al., 2012; Luhmann et al., 2012; Birk et al., 2014). Unlike chemical modification, the degree of thermal modification depends on the timescale of recharge variations. Shorter, storm-event thermal perturbations provide maximum information about conduits with hydraulic diameters on the meter scale; longer, seasonal thermal perturbations probe smaller, mm- to cm-scale flow paths (Covington et al., 2012). Previous work has also demonstrated that groundwater input into surface streams in karst terrains modifies the relationships between air and water temperatures (O'Driscoll and DeWalle, 2006). The extent of this modification will depend upon whether groundwater has had sufficient residence time to reach thermal equilibration (Luhmann et al., 2011; Covington et al., 2012).

In addition to correlations between thermal signals and conduit geometry, temperature peaks have been used as a simple and inexpensive means to estimate residence times within karst conduit systems when the timing of changes in recharge temperature is known ~~(Martin and Dean, 1999; Birk et al., 2004; Screaton et al., 2004; Covington et al., 2011)~~ (Mart However, since heat exchange within a karst conduit introduces a retardation in the timing of the peak, residence times estimated using temperature will typically be longer than the true residence time. The magnitude of this error, and its functional relationship to conduit geometry and boundary conditions, have not been previously quantified, though Birk et al. (2004) noted that estimates of conduit volume based on temperature lags displayed significantly more scatter than estimates using electrical conductivity lags, and concluded that electrical conductivity provided a more reliable means of estimating travel times.

Recent work used temperature to identify water sources by employing a two component mixing model (Doucette and Peterson, 2014). However, since heat exchange within a karst conduit dampens all thermal perturbations, there will be error in estimates of different water source fractions derived from models that assume conservative endmember temperatures. Temperature mixing models will typically ~~ovestimate~~ overestimate contributions from background temperature sources and underestimate source waters that provide the thermal perturbations at the thermal peak/trough. Alternatively, during the thermal recession, the heated or cooled rock surrounding the conduit may potentially facilitate water temperatures that are no longer within the temperature range of the different water sources. The magnitude of these errors will depend upon the extent of water temperature change that occurs along the flow paths.

Our primary objective in this study is to demonstrate the effect of conduit geometry on thermal damping and retardation in karst conduits using both analytical solutions and numerical simulations. We also consider the effects of fluid flow velocity, recharge characteristics, and rock and water physical properties. A relationship between conduit geometry and thermal damping or retardation may ultimately be used to estimate conduit diameter given recharge temperature and down-gradient monitoring data that includes water temperature and a conservative tracer. These relationships can also be used to estimate, and potentially correct for, errors in residence times or water source fractions derived from temperature pulses, and to understand how these errors vary with conduit properties and recharge.

2 Conceptual model

A simplified conceptual model of heat transport in a conduit through a karst aquifer is employed to provide a general understanding of thermal damping and retardation in karst conduits. Heat transport occurs via advection and dispersion in the conduit, conduction in the rock surrounding the conduit, and exchange between the conduit and rock. Both a circular conduit and a planar fracture or bedding plane are investigated. Velocity is imposed along the entire length of the conduit, and the following analysis generally assumes a number of constants to simplify the system, including water flow at a constant velocity in a conduit with a constant hydraulic diameter. However, the effects of velocity variations induced by recharge events and a conduit diameter that varies along its length are briefly considered. The analysis also generally employs conduits with full pipe flow, but open channel flow, where conduits are only partially full of water, is also considered in a few example cases. The conceptual model does not account for exchange of water between the conduit and matrix (or fractures or other conduits) or spatial velocity gradients or mobile/immobile regions within the conduit. Finally, the analysis employs a number of simple functions to approximate the shape of thermal perturbations produced in nature. Some limitations of our conceptual model are discussed in Sect. 9.2.

3 Mathematical model

Temperature along a karst conduit as a function of time can be approximated by the 1-D heat advection-dispersion equation:

$$\frac{\partial T_\mathrm{w}}{\partial t} = D_\mathrm{L}\frac{\partial^2 T_\mathrm{w}}{\partial x^2} - V\frac{\partial T_\mathrm{w}}{\partial x} + \frac{4h_\mathrm{conv}}{\rho_\mathrm{w} c_{p,\mathrm{w}} D_\mathrm{H}}(T_\mathrm{s} - T_\mathrm{w}), \tag{1}$$

where T_w is the water temperature, t is time, D_L is the longitudinal dispersivity, x is the longitudinal distance down the conduit, V is the water velocity, h_conv is the convective heat transfer coefficient, ρ_w is the density of water, $c_{p,\mathrm{w}}$ is the specific heat of water at constant pressure, D_H is the hydraulic diameter of the flow path, and T_s is the conduit wall surface temperature. The terms on the right side of Eq. (1) describe heat dispersion, heat advection, and heat exchange with the surrounding rock. The convective heat transfer coefficient is given by

$$h_\mathrm{conv} = \frac{k_\mathrm{w}\mathrm{Nu}}{D_\mathrm{H}}, \tag{2}$$

where k_w is the thermal conductivity of water and Nu is the dimensionless Nusselt number, which is the ratio of convective to purely conductive heat transfer through the convective boundary layer near the wall. Nu for turbulent flow is given by the empirically derived Gnielinski correlation (Incropera et al., 2007, Eq. 8.62),

$$1 + 12.7(f/8)^{1/2}(\mathrm{Pr}^{2/3} - 1), \tag{3}$$

where f is the Darcy–Weisbach friction factor, ~~$Re = \rho_{\mathrm{w}} V D_{\mathrm{H}} / \mu_{\mathrm{w}}$~~ $\mathrm{Re} = \rho_{\mathrm{w}} V D_{\mathrm{H}} / \mu_{\mathrm{w}}$ is the dimensionless Reynolds number, $\mathrm{Pr} = c_{p,\mathrm{w}} \mu_{\mathrm{w}} / k_{\mathrm{w}}$ is the dimensionless Prandtl number of water, and μ_{w} is the dynamic viscosity of water.

Conduction provides a strong control over heat exchange in karst conduits (Covington et al., 2011). Heat conduction in the rock surrounding a circular conduit with no energy generation can be described, using cylindrical symmetry, by the 2-D heat conduction equation:

$$\frac{1}{r}\frac{\partial}{\partial r}\left(r\frac{\partial T_{\mathrm{r}}}{\partial r}\right) + \frac{\partial^2 T_{\mathrm{r}}}{\partial x^2} = \frac{1}{\alpha_{\mathrm{r}}}\frac{\partial T_{\mathrm{r}}}{\partial t}, \tag{4}$$

where r is the radial distance from the conduit center, T_{r} is the rock temperature, and $\alpha_{\mathrm{r}} = k_{\mathrm{r}}/(\rho_{\mathrm{r}} c_{\mathrm{p,r}})$ is the here-assumed isotropic and homogeneous thermal diffusivity of rock, with k_{r} denoting the thermal conductivity, ρ_{r} the density, and $c_{\mathrm{p,r}}$ the specific heat. To represent heat transport in rock adjacent to a planar fracture or a bedding plane parting, we use translational symmetry, and the heat conduction equation becomes

$$\frac{\partial^2 T_{\mathrm{r}}}{\partial y^2} + \frac{\partial^2 T_{\mathrm{r}}}{\partial x^2} = \frac{1}{\alpha_{\mathrm{r}}}\frac{\partial T_{\mathrm{r}}}{\partial t}, \tag{5}$$

where y is the distance from the fracture center. Furthermore, heat exchange in a cylindrical conduit can be approximated by heat exchange in planar coordinates in many cases (Covington et al., 2011) , permitting simpler planar simulations.

The boundary conditions are:

$$\left.\frac{\partial T_{\mathrm{w}}}{\partial x}\right|_{x=\text{ conduit outlet}} = 0, \tag{6}$$

$$\frac{\partial T_{\mathrm{r}}}{\partial r} \to 0 \text{ as } r \to \infty, \tag{7}$$

and

$$k_{\mathrm{r}}\left.\frac{\partial T_{\mathrm{r}}}{\partial r}\right|_{r=\text{ conduit wall}} = h_{\mathrm{conv}}(T_{\mathrm{s}} - T_{\mathrm{w}}). \tag{8}$$

In planar coordinates, r in Eqs. (7) and (8) is replaced by y:

$$\frac{\partial T_\mathrm{r}}{\partial y} \to 0 \text{ as } y \to \infty, \tag{9}$$

$$k_\mathrm{r} \left.\frac{\partial T_\mathrm{r}}{\partial y}\right|_{y = \text{ conduit wall}} = h_\mathrm{conv}(T_\mathrm{s} - T_\mathrm{w}). \tag{10}$$

4 Analytical solutions for damping and thermal retardation

Simplification of Eq. (1) allows derivation of several useful analytical solutions. Karst conduits are frequently advection-dominated, with Peclet Numbers of around 100 (Field and Nash, 1997). Therefore, neglection of longitudinal dispersivity will provide a reasonable approximation in many cases. This approximation will break down for particularly short duration pulses (Hauns et al., 2001), but is more likely to hold for the longer term pulses typically found from natural perturbations. Neglecting longitudinal dispersivity results in

$$\frac{\partial T_\mathrm{w}}{\partial t} = -V \frac{\partial T_\mathrm{w}}{\partial x} + \frac{4 h_\mathrm{conv}}{\rho_\mathrm{w} c_{p,\mathrm{w}} D_\mathrm{H}} (T_\mathrm{s} - T_\mathrm{w}). \tag{11}$$

For most relevant cases, where the timescale of the change in water temperature is not extremely short, the approximation $h_\mathrm{conv} \to \infty$ is valid (Covington et al., 2011). In this case heat flow is limited by conduction in the rock, and one obtains a boundary condition

$$T_\mathrm{r}\left(x, r \text{ or } y = \text{ conduit wall}, t\right) = T_\mathrm{w}(x,t). \tag{12}$$

4.1 Sinusoidal solution for the planar case

Heat conduction in the rock along the length of the conduit (the x direction) is neglected, and thus, the equation for heat conduction in the rock becomes

$$\frac{\partial^2 T_\mathrm{r}(x,y,t)}{\partial y^2} = \frac{1}{\alpha_\mathrm{r}} \frac{\partial T_\mathrm{r}(x,y,t)}{\partial t}. \tag{13}$$

4.2 ~~Sinusoidal solution for the planar case~~

Equations (10) to (13) can be solved for the case of sinusoidally varying water temperature, allowing direct calculation of the thermal damping and retardation of the input wave. The retardation and damping produced for this sinusoidal upstream boundary condition provide significant insight into the response from many pulses found in natural settings, including, as will be seen later, a single isolated pulse. For the sinusoidal solution, we employ a shifted temperature variable defined as

$$T'_{\mathrm{r}} = T_{\mathrm{r}} - T_{\mathrm{r},\infty}, \tag{14}$$

where $T_{\mathrm{r},\infty}$ is the rock temperature at an infinite distance from the conduit axis. For an upstream boundary condition that is sinusoidal in time, the solution for the rock temperature is separable and has the functional form

$$T'_{\mathrm{r}}(x,y,t) = X(x)Y(y)T'_t(t). \tag{15}$$

Since the water and rock temperatures are assummed equal at the boundary (Eq. 12), Eq. (15) contains all of the temperature field. With a sinusoidal upstream boundary condition, the time varying component of the solution is also sinusoidal, $T'_t(t) = T'_{\mathrm{w,in}}e^{-i\omega t}$ and $T'_{\mathrm{r}}(x,y,t) = T'_{\mathrm{w,in}}X(x)Y(y)e^{-i\omega t}$, where $T'_{\mathrm{w,in}}$ is the amplitude of the input temperature variation. Using this in Eq. (13), combined with the boundary condition that $\lim_{y\to\infty} T'_{\mathrm{r}} = 0$, leads to

$$Y(y) = e^{(-1+i)\sqrt{\frac{\omega}{2\alpha_{\mathrm{r}}}}y}. \tag{16}$$

The function $X(x)$, can then be derived using Eqs. (10)–(12) leading to

$$X(x)Y(y)\frac{\mathrm{d}T'_t(t)}{\mathrm{d}t} = -VY(y)T'_t(t)\frac{\mathrm{d}X(x)}{\mathrm{d}x} + \frac{4\alpha_{\mathrm{r}}}{\Psi D_{\mathrm{H}}}X(x)T'_t(t)\left.\frac{\mathrm{d}Y(y)}{\mathrm{d}y}\right|_{y=\text{ conduit wall}}, \tag{17}$$

where $\Psi = \rho_{\mathrm{w}}c_{p,\mathrm{w}}/(\rho_{\mathrm{r}}c_{\mathrm{p,r}})$ is a ratio of the volumetric heat capacities of water and rock. This is an ordinary differential equation with constant coefficients and the solution is an exponential function $X(x) = e^{-\gamma x}$, where

$$\gamma = -i\frac{\omega}{V} - (-1+i)\frac{4}{V\Psi D_\mathrm{H}}\sqrt{\frac{\alpha_\mathrm{r}\omega}{2}}e^{(1-i)\sqrt{\frac{\omega}{2\alpha_\mathrm{r}}}y}. \tag{18}$$

For the water temperature at the conduit outlet, $T'_\mathrm{w,out}$, this gives the solution

$$T'_\mathrm{w,out}(t) = T'_\mathrm{w,in}\exp\left[-i\omega t + i\frac{\omega}{V}L + (i-1)\frac{4L}{V\Psi D_\mathrm{H}}\sqrt{\frac{\alpha_\mathrm{r}\omega}{2}}\right]. \tag{19}$$

Since we are interested only in real solutions, we fix the phase and only look at the real part of the equation.

From this solution, one can directly derive both the retardation and damping experienced by each sinusoidal temperature peak. A peak in the output temperature is reached at a distance L (i.e., conduit length) downstream of the input at the time, $t_\mathrm{peak,out}$, when the imaginary part of the exponent is zero, that is,

$$-\omega t_\mathrm{peak,out} + \frac{\omega}{V}L + \frac{4L}{V\Psi D_\mathrm{H}}\sqrt{\frac{\alpha_\mathrm{r}\omega}{2}} = 0. \tag{20}$$

The fluid flow-through time through the conduit is $t_\mathrm{ft} = L/V$, and the retardation of the thermal peak, τ, is the difference

$$\tau = t_\mathrm{peak,out} - t_\mathrm{ft} = \frac{4L}{V\Psi D_\mathrm{H}}\sqrt{\frac{\alpha_\mathrm{r}}{2\omega}}. \tag{21}$$

As can been seen from the real part of γ, the damping of the upstream temperature peaks observed at the downstream end of the conduit ($x = L$) is given by

$$\frac{T'_\mathrm{w,out}}{T'_\mathrm{w,in}} = \exp\left[-\frac{4L}{V\Psi D_\mathrm{H}}\sqrt{\frac{\alpha_\mathrm{r}\omega}{2}}\right]. \tag{22}$$

This solution illustrates a thermal length scale, $\lambda_{\mathrm{T,sin}}$, that is appropriate for sinusoidal temperature variations in the input temperature, with

$$\lambda_{\mathrm{T,sin}} = \frac{V \Psi D_{\mathrm{H}}}{4} \sqrt{\frac{2}{\alpha_{\mathrm{r}} \omega}}. \tag{23}$$

$\lambda_{\mathrm{T,sin}}$ is, to within a dimensionless factor of order one, equivalent to the late time thermal length scale of Eq. (22) in Covington et al. (2012).

4.2 Sinusoidal solution for the cylindrical case

For heat conduction within the rock in the vicitinity of a karst conduit with a cylindrical geometry, we again neglect conduction in the direction along the conduit (x) and instead of Eq. (4) we use

$$\frac{\partial^2 T_{\mathrm{r}}(x,r,t)}{\partial r^2} + \frac{1}{r} \frac{\partial T_{\mathrm{r}}(x,r,t)}{\partial r} = \frac{1}{\alpha_{\mathrm{r}}} \frac{\partial T_{\mathrm{r}}(x,r,t)}{\partial t}. \tag{24}$$

The solution remains separable such that

$$T'_{\mathrm{r}}(x,r,t) = X(x) R(r) T'_t(t). \tag{25}$$

Again we use sinusoidal $T'_t(t)$ and get $T'_{\mathrm{r}}(x,r,t) = T'_{\mathrm{w,in}} X(x) R(r) e^{-i\omega t}$. Substituting this into Eq. (24) gives a Bessel equation whose solutions are Bessel functions. ~~The boundary condition~~ From the boundary condition $\lim_{r\to\infty} T'_{\mathrm{r}} = 0$ follows $\lim_{r\to\infty} R(r) = 0$, which limits the solution space for $R(r)$ to specific linear combinations of Bessel functions that are known as Hankel functions of the first kind, $H_i^{(1)}$. The solution is

$$R(r) = \frac{H_0^{(1)}\left((1+i)\sqrt{\frac{\omega}{2\alpha_{\mathrm{r}}}} r\right)}{H_0^{(1)}\left((1+i)\sqrt{\frac{\omega}{2\alpha_{\mathrm{r}}}} D_{\mathrm{H}}/2\right)}. \tag{26}$$

As in the planar case, $X(x)$ is obtained from Eq. (11) and has the form $X(x) = e^{-\gamma x}$, where

$$\gamma = -i\frac{\omega}{V} + (i+1)\,\frac{\sqrt{2\alpha_\mathrm{r}\omega}}{\Psi D_\mathrm{H}/2}\,\frac{H_1^{(1)}\left((1+i)\sqrt{\frac{\omega}{2\alpha_\mathrm{r}}}D_\mathrm{H}/2\right)}{H_0^{(1)}\left((1+i)\sqrt{\frac{\omega}{2\alpha_\mathrm{r}}}D_\mathrm{H}/2\right)}. \tag{27}$$

Because of the special functions, this solution is less useful analytically, but provides a straightforward means of calculating the output wave numerically.

5 Numerical integration of the planar case for arbitrary recharge temperature

As shown above, if the temperature at the input is $T_\mathrm{w,in}(t) = e^{-i\omega t}$ then the temperature at the output is $T_\mathrm{w,out}(t) = T_\mathrm{w,in}(t)X(L) = e^{-\gamma(\omega)L - i\omega t}$. A general $T_\mathrm{w,in}(t)$ can be expressed in terms of its Fourier transform,

$$T_\mathrm{w,in}(t) = \int_{-\infty}^{\infty} K(\omega)e^{-i\omega t}\mathrm{d}\omega, \tag{28}$$

and the output temperature is then calculated as

$$T_\mathrm{w,out}(t) = \int_{-\infty}^{\infty} K(\omega)e^{-\gamma(\omega)L - i\omega t}\mathrm{d}\omega. \tag{29}$$

A Gaussian pulse is of particular interest, since this shape approximates many natural recharge events and is also the functional form we use for the simulations below. We use a Gaussian recharge function of the form

$$T_\mathrm{w,in}(t) = T_\mathrm{r,0} + \mathcal{R}_\mathrm{A} e^{-\frac{(t - t_\mathrm{peak,in})^2}{2\sigma^2}}, \tag{30}$$

where $T_{\mathrm{w,in}}$ is T_{w} at $x=0$, $T_{\mathrm{r},0}$ is the initial rock temperature (or ~~rock temperature at infinity~~$T_{\mathrm{r},\infty}$), $\mathcal{R}_{\mathrm{A}}$ is the recharge temperature amplitude, $t_{\mathrm{peak,in}}$ is the peak time at $x=0$, and σ controls the width of the thermal pulse.

The Fourier transform is given by

$$K(\omega)=\delta(\omega)+\frac{\mathcal{R}_{\mathrm{A}}c}{\sqrt{2\pi}}e^{-\frac{c^2\omega^2}{2}+it_{\mathrm{peak,in}}\omega}. \tag{31}$$

Therefore the general solution for a Gaussian pulse can be calculating using the integral

$$T_{\mathrm{w,out}}(t)=1+\frac{\mathcal{R}_{\mathrm{A}}c}{\sqrt{2\pi}}\int\limits_{-\infty}^{\infty}e^{-\frac{c^2\omega^2}{2}+it_{\mathrm{peak,in}}\omega}e^{-\frac{L}{\Psi D_{\mathrm{H}}/2}\sqrt{\frac{\alpha_{\mathrm{r}}}{2}}\sqrt{\omega}+i\left(\frac{L}{\Psi D_{\mathrm{H}}/2}\sqrt{\frac{\alpha_{\mathrm{r}}}{2}}\sqrt{\omega}+\left(\frac{L}{V}-t\right)\omega\right)}\mathrm{d}\omega. \tag{32}$$

In practice, this equation, or Eq. (29) for the general case, must be integrated numerically. However, the Fourier transform solution provides an efficient means of numerically calculating thermographs.

6 Numerical simulations

In order to relax the somewhat restrictive assumptions required by the analytical solutions, and particularly to test the applicability of the sinusoidal analytical solutions to the propagation of isolated pulses, we present the results of numerical simulations of thermal pulses. These simulations solve the full version of Eqs. (1) and (4) or (5) for a variety of recharge and flow conditions, conduit geometries, thermal pulse shapes, rock and water physical properties, and also for open channel cases that include radiative heat exchange. For the majority of the simulation set, recharge temperature is varied according to the Gaussian function given in Eq. (30). For each simulation, σ is defined to attain a desired recharge duration, $\mathcal{R}_{\mathrm{D}}$, or full width at half maximum given by

$$\mathcal{R}_{\mathrm{D}}=2\sigma\sqrt{2\ln 2}. \tag{33}$$

For the initial condition, T_w and T_r are set equal to ~~T_r at infinity or $T_\mathrm{w}(x,t=0)=T_\mathrm{r}(r,t=0)=10\,^\circ\mathrm{C}$~~$T_{\mathrm{r},\infty}$ or $T_\mathrm{w}(x,t=0)=T_\mathrm{r}(x,r$ or $y,t=0)=10\,^\circ\mathrm{C}$.

For most of the simulations, V is constant, although V varies between different simulations. f is approximated for most simulations using the von Kármán Equation,

$$f=[1.74+2\log(R/\epsilon)]^{-2}, \tag{34}$$

where $R=D_\mathrm{H}/2$ is the conduit radius and ϵ is the roughness height (i.e., the average distance that irregularities on the rock wall protrude into the conduit). We set $\epsilon=2.15\,\mathrm{cm}$ for all simulations. We also run simulations where f is calculated using the empirical Colebrook-White Equation, and we find that simulation results are identical regardless of the equation used to determine f (Luhmann, 2011).

The finite element package COMSOL Multiphysics® (Version 3.5) is used to numerically solve the coupled heat advection-dispersion and conduction equations. Using the Coefficient Form PDE mode in COMSOL, Eq. (1) is solved along a 1-D line, which represents a conduit (Fig. 1a) or fracture (Fig. 1b). Because of axial symmetry, a simulation of conduction in the rock surrounding a circular conduit with full pipe flow may be reduced to a 2-D axisymmetric problem. Thus, Eq. (4) is solved using COMSOL's Conduction Heat Transfer application mode with a 2-D axisymmetric rectangle for cylindrical simulations (Fig. 1a). Similarly, because of translational symmetry across the fracture plane, a simulation of conduction in the rock surrounding a water-filled fracture may be simplified to a 2-D planar problem. Thus, Eq. (5) is solved in a 2-D rectangle in Cartesian coordinates for planar simulations (Fig. 1b). The 1-D line and either the 2-D cylindrical or planar rectangle are coupled to each other at one of the rectangle edges using the Extrusion Coupling Variables feature in COMSOL. The 1-D conduit or fracture line and the rock at the conduit or fracture wall were discretized into 1000 finite elements along the flow path length for all simulations. Mesh resolution gradually coarsens in the 2-D rectangle of rock away from the flow path wall, but the 2-D rectangle was generally discretized into 23 000 elements. COMSOL uses an implicit method to solve the system of equations. User-defined relative and absolute tolerances are compared to the estimated error to modify timestep duration to obtain the desired accuracy. The relative and absolute tolerances were set to $\leq 10^{-6}$ and $\leq 10^{-7}$, respectively. Several example cases were run at higher spatial and temporal resolution and produced the same results.

We conduct numerous simulations where we vary the parameters to consider their effect on thermal damping and retardation. Table 1 lists default values for parameters, but simulations were also run with other values, which are provided in the Supplement. The thermal transmission factor, F, which provides a means to quantify damping, is given by

$$F = \frac{T_{\mathrm{w,peak,out}} - T_{\mathrm{r},\infty}}{T_{\mathrm{w,peak,in}} - T_{\mathrm{r},\infty}}, \tag{35}$$

where $T_{\mathrm{w,peak,out}}$ is the outlet peak water temperature and $T_{\mathrm{w,peak,in}}$ is the inlet peak water temperature. The thermal peak retardation, τ, for each simulation is the time of peak temperature at the outlet minus the flow-through time (Eq. 21). Though the notation here is in terms of temperature peaks, the same equations apply to temperature troughs. τ and F for all simulations are provided in the Supplement.

7 Results

7.1 Thermal damping

The damping of temperature peaks in the simulations ~~shows a dependence~~ is dependent on the ratio $L/\lambda_{\mathrm{T,sin}}$. When the ratio $L/\lambda_{\mathrm{T,sin}}$ is small, there is little damping of recharge signals. However, when the ratio $L/\lambda_{\mathrm{T,sin}}$ is large, recharge signals undergo significant to complete damping. For the planar sinusoidal solution, the transmission factor, F, is given by Eq. (22). In order to compare this analytical solution for damping of sinusoids with the simulations that contain Gaussian input thermographs, we need an approximate conversion between angular frequency of the sinusoid, ω, and an appropriate analog for the Gaussian pulse. We use the relation $\omega = \pi/(C_{\mathrm{time}}\mathcal{R}_{\mathrm{D}})$, which relates the period of the sinusoid to a multiple of the full width at half maximum of the Gaussian curve. The time conversion constant, C_{time}, is treated as a fitting parameter. Using this approximation, and the definition of the transmission factor

(Eq. 35), Eq. (22) can be rewritten as

$$F_{\text{planar}} = \exp\left(-\frac{4L}{V\Psi D_{\text{H}}}\sqrt{\frac{\pi\alpha_{\text{r}}}{2C_{\text{time}}\mathcal{R}_{\text{D}}}}\right). \tag{36}$$

For the planar simulations, and cylindrical simulations that are well-approximated with the planar solution, we find that a value of $C_{\text{time}} \approx 4$ provides a tight fit to the transmission factors measured from the pulses in the simulations (Fig. 2). Covington et al. (2011) showed that the agreement between planar and cylindrical heat transport solutions was dependent on a dimensionless number, $\Theta = (R^2\overline{V})/(L\alpha_{\text{r}})$, where $\overline{V}$ is a time-averaged or reference flow velocity, with cylindrical cases well-approximated by the planar solution for $\Theta \gtrsim 10$. Similarly, here we find that Eq. (36) breaks down for cylindrical simulations with small Θ. However, we also find that the error is strongly correlated to Θ, and the damping in the cylindrical cases is well-fit by a correction factor of the form

$$F_{\text{cyl}} = \frac{\Theta}{C_{\text{cyl}} + \Theta} F_{\text{planar}}. \tag{37}$$

This correction factor, with a value of $C_{\text{cyl}} \approx 0.4$, roughly accounts for the additional heat exchange. Though an approximation of the cylindrical solution given in Sect. 4.2 might provide a more well-motivated correction, this equation produces acceptable results and is simpler to implement since it requires no calculation of Hankel functions. Figure 2 shows a comparison between the transmission factors within the simulations and the values of F_{planar} or F_{cyl} for the planar and cylindrical simulations, respectively.

7.2 Thermal retardation

As for thermal damping, the thermal retardation of a Gaussian pulse can be approximated using the form of the sinusoidal solution along with a multiplicative time constant. For thermal retardation, we find that Eq. (21) provides a good approximation to the simulated cases (Fig. 3) with a choice of $\omega \approx \pi/\mathcal{R}_{\text{D}}$, such that

$$\tau_{\text{planar}} = \frac{4L}{V\Psi D_{\text{H}}}\sqrt{\frac{\alpha_{\text{r}}\mathcal{R}_{\text{D}}}{2\pi}}. \tag{38}$$

While this relation provides an excellent fit to the planar cases, and most of the cylidrical cases, cylindrical cases with small values of Θ do produce some scatter. This scatter is sufficiently small that we do not attempt to develop a correction for it. There is also some scatter associated with simulations with relatively slow velocities. This scatter is likely caused by numerical dispersion.

7.3 Relaxation of additional assumptions

Our anlaysis thus far, including the simulations, employs a number of simplifications or approximations, such as constant conduit diameter and constant flow velocity. Here, we run simulations that relax these assumptions to examine potential uncertainty in the F and τ relationships. We consider the effect of variable diameter or flow velocity within an individual conduit and also run open channel simulations, where a conduit is only partially filled with water and radiative heat exchange occurs. Finally, we consider other functions that approximate the shape of recharge thermographs in nature, to examine whether different shapes produce significantly different values of damping or retardation.

7.3.1 Variable hydraulic diameter

The conduit hydraulic diameter, D_{H}, typically changes along a karst flow path. If this occurs, the thermal signal at the monitoring location of interest will be a composite signal, and estimates of D_{H} using Eqs. (36) and (38) will then be estimates of an effective hydraulic diameter, $D_{\mathrm{H,e}}$, that is some function of the different size flow paths that the water traversed. If the pulse undergoes little modification in shape or duration as it flows through different conduit segments, then the total transmission factor, F_{T}, in a conduit with multiple segments with different values of D_{H}, is given by

$$F_{\mathrm{T}} = \prod_{i=1}^{n} F_i, \tag{39}$$

where F_i is the transmission factor from segment i. Furthermore, the total retardation of the thermal peak, τ_T, is given by

$$\tau_\mathrm{T} = \sum_{i=1}^{n} \tau_i, \tag{40}$$

where τ_i is the retardation from segment i. τ_i is given by

$$\tau_i = \left[\frac{4}{\Psi}\sqrt{\frac{\alpha_\mathrm{r}\mathcal{R}_\mathrm{D}}{2\pi}}\right]\frac{L_i}{V_i D_{\mathrm{H},i}}, \tag{41}$$

where the quantity in square brackets is approximately constant and L_i, V_i, and $D_{\mathrm{H},i}$ are the length, velocity, and hydraulic diameter, respectively, of segment i. It follows that

$$\tau_\mathrm{T} = \left[\frac{4}{\Psi}\sqrt{\frac{\alpha_\mathrm{r}\mathcal{R}_\mathrm{D}}{2\pi}}\right]\sum_{i=1}^{n}\frac{L_i}{V_i D_{\mathrm{H},i}}. \tag{42}$$

We can define an effective length (L_e), velocity (V_e), and diameter ($\cancel{D_\mathrm{e}}D_\mathrm{H,e}$) such that

$$\tau_\mathrm{T} = \left[\frac{4}{\Psi}\sqrt{\frac{\alpha_\mathrm{r}\mathcal{R}_\mathrm{D}}{2\pi}}\right]\frac{L_\mathrm{e}}{V_\mathrm{e} D_\mathrm{H,e}}. \tag{43}$$

From this we can see that, given the quantities in the square bracket are constant, the response of a multi-diameter conduit is the same as that of an equivalent single diameter conduit with the effective length, velocity, and diameter. We can then consider the relationship of $D_\mathrm{H,e}$ to $D_{\mathrm{H},i}$ as well as the relationship of L_e to L_i. There is more than one equivalent conduit that can be defined depending upon the constraints chosen. We impose the following four constraints, which we deem to be the most physically meaningful:

1. The retardation of the equivalent conduit is equal to that of the multiple segment conduit,

$$\frac{L_\mathrm{e}}{V_\mathrm{e} D_\mathrm{H,e}} = \sum_{i=1}^{n}\frac{L_i}{V_i D_{\mathrm{H},i}}. \tag{44}$$

2. Mass (discharge) is conserved along the multiple segment conduit,

$$V_i D_{\mathrm{H},i}^2 = V_{i+1} D_{\mathrm{H},i+1}^2. \tag{45}$$

3. The multiple segment and equivalent conduits have the same discharge,

$$V_\mathrm{e} D_{\mathrm{H,e}}^2 = V_i D_{\mathrm{H},i}^2. \tag{46}$$

4. The flow-through time of the multiple segment and equivalent conduits is the same,

$$\frac{L_\mathrm{e}}{V_\mathrm{e}} = \sum_{i=1}^{n} \frac{L_i}{V_i}. \tag{47}$$

Using these constraints, it is possible to solve for the equivalent diameter and length,

$$D_{\mathrm{H,e}} = \frac{\sum\limits_{i=1}^{n} L_i D_{\mathrm{H},i}^2}{\sum\limits_{i=1}^{n} L_i D_{\mathrm{H},i}} = \frac{(\text{Total Conduit Volume})}{\sum\limits_{i=1}^{n} (i\text{th Segment Volume})/D_{\mathrm{H},i}} = \frac{t_\mathrm{ft}}{\sum\limits_{i=1}^{n} t_{\mathrm{ft},i}/D_{\mathrm{H},i}} \tag{48}$$

and

$$L_\mathrm{e} = \sum_{i=1}^{n} \frac{L_i D_{\mathrm{H},i}^2}{D_{\mathrm{H,e}}^2} = \frac{(\text{Total Conduit Volume})}{(\text{Equivalent Conduit Cross Sectional Area})}. \tag{49}$$

The relationships between the equivalent model parameters and conduit volumes or flow-through times assume that the relationship between hydraulic diameter and cross sectional area is fixed. An analogous derivation using transmission factor, F, rather than retardation, τ, yields the same relationships, and therefore the equivalent models for damping and retardation are the same.

The equivalent diameter is given by the volume- or time-weighted harmonic mean of the hydraulic diameters of the individual segments. Since the harmonic mean accentuates the smaller values in a set, and is always less than the arithmetic mean, one might think that the smaller diameters figure more heavily in the calculation of an equivalent diameter. However, this effect is offset by the weighting by volume, or, equivalently, flow-through time. For the same length, larger diameter conduits will have larger volumes and longer flow-through times. The effect of the weighting is sufficiently strong that, for two conduit segments of ~~equivalent~~ equal length, the equivalent diameter is more heavily weighted toward the larger diameter.

Since discharge and flow-through time are fixed, the volumes of the multi-segment and equivalent conduits must be the same. Consequently, the length of the equivalent model is equal to this volume divided by the cross-sectional area of the equivalent model conduit. While one might like to hold conduit length fixed between the multi-segment and equivalent models, this is not possible given the constraints (1–4) used above, and we deem these constraints to be more physically meaningful than holding length constant. This is, however, a somewhat arbitrary choice and other equivalent models could also be derived. As an example of the relationship between multiple segment and equivalent conduit properties, Fig. 4 shows the ratio of $D_{\mathrm{H,e}}$ to the average hydraulic diameter, $D_{\mathrm{H,avg}}$, and the ratio of L_{e} to $L_1 + L_2$ for systems containing two conduit segments with equal length.

Simulations ~~were~~ are run in cylindrical coordinates to test if a conduit with two segments with different diameters and a conduit with a constant effective diameter calculated from Eqs. (48) and (49) produce the same transmission and retardation. We run two example cases of a multiple segment conduit, both of which have two segments with equal lengths and different diameters. In one case D_{H} increases by 20 % halfway down the conduit and in the other case by 100 %. Table 2 provides values of model parameters for each case and the transmission and retardation ~~measured~~ from each simulated thermograph. For the simulations of a conduit with two different D_{H} segments, the output of the first section was used as input into the second section. For the two example cases, there is good agreement between the transmission factors and retardation observed in the multi-segment and equivalent models (Table 2).

7.3.2 Variable flow velocity

During recharge events, discharge variability causes variations in flow velocity, V. To explore the effect of varying velocity on the amount of damping and retardation that occurs, we ~~ran~~ run additional simulations in cylindrical coordinates where velocity was varied and compared them with constant velocity simulations. For each variable velocity simulation, both V and $T_{\mathrm{w,in}}$ are defined by a Gaussian equation of the form of Eq. (30). Both curves use the same $t_{\mathrm{peak,in}}$ and σ, but the initial velocity, V_0, and velocity amplitude, V_{A}, (equivalent to $T_{\mathrm{r},0}$ and $\mathcal{R}_{\mathrm{A}}$, respectively, in Eq. 30) are both set to $0.1\,\mathrm{m\,s^{-1}}$ for all simulations. This simulates a velocity that ranges from 0.1 to $0.2\,\mathrm{m\,s^{-1}}$ over the duration of the pulse. In these simulations velocity and input temperature began to change at the same time, and the peak water temperature at the input occurs at the same time as the peak velocity in the conduit. Because these are 1-D simulations of full pipe flow, there are no spatial velocity gradients, even though velocity varies as a function of time. We also ~~ran~~ run equivalent constant velocity simulations, where the flow velocity for each simulation ~~was set to the average velocity that occurred while the thermal peak was in the conduit during~~ is set so that the flow-through time is equal to the flow-through time of the corresponding variable velocity simulation. Five sets of simulations ~~were~~ are run to compare five different recharge duration, $\mathcal{R}_{\mathrm{D}}$, to flow-through time ratios, L/V.

Table 3 provides transmission and retardation data for simulations that consider the effect of variable velocity. For most cases, each set of variable V and constant V simulations produced similar damping. However, as the ratio of recharge duration to flow-through time decreased, the constant V simulations underwent somewhat more damping than variable V simulations. In general, thermal retardation values were similar for the constant and variable V simulations. However, thermal peaks from variable V simulations are characterized by more retardation than the constant V cases when $\mathcal{R}_{\mathrm{D}} \lesssim L/V$ and less retardation when $\mathcal{R}_{\mathrm{D}} > L/V$. The fraction of time spent at a velocity above or below the average velocity ultimately controlled whether variable V simulations produced less or more retardation, respectively, than the corresponding constant V simulation. The maximum difference between thermal retardation observed in the constant and variable V simulations is approximately 30 %.

7.3.3 Open channel

If water flows along a conduit with a free surface, then a potentially significant amount of heat exchange occurs via radiation through the air. The significance of this exchange is a function of the time scale of the pulse (Covington et al., 2011). To incorporate radiation, we add one more term to the heat advection-dispersion equation:

$$\frac{\partial T_\mathrm{w}}{\partial t} = D_\mathrm{L}\frac{\partial^2 T_\mathrm{w}}{\partial x^2} - V\frac{\partial T_\mathrm{w}}{\partial x} + \frac{4h_\mathrm{conv}}{\rho_\mathrm{w} c_{p,\mathrm{w}} D_\mathrm{H}}(T_\mathrm{s,w} - T_\mathrm{w}) + \frac{4h_\mathrm{rad} A_\mathrm{d}}{\rho_\mathrm{w} c_{p,\mathrm{w}} D_\mathrm{H} A_\mathrm{w}}(T_\mathrm{s,d} - T_\mathrm{w}), \tag{50}$$

where $T_\mathrm{s,w}$ is the wet conduit wall surface temperature, h_rad is the radiative heat transfer coefficient, $A_\mathrm{d} = P_\mathrm{d}/W_\mathrm{fs}$ is the ratio of dry conduit perimeter (P_d) to the width of the water's free surface (W_fs), $A_\mathrm{w} = P_\mathrm{w}/W_\mathrm{fs}$ is the ratio of wet conduit perimeter (P_w) to W_fs, and $T_\mathrm{s,d}$ is the dry conduit wall surface temperature. h_rad is given by

$$h_\mathrm{rad} = \frac{\sigma_\mathrm{SB}}{A_\mathrm{d}}(T_\mathrm{w} + T_\mathrm{s,d})\left(T_\mathrm{w}^2 + T_\mathrm{s,d}^2\right), \tag{51}$$

where $\sigma_\mathrm{SB} = 5.67 \times 10^{-8}\,\mathrm{W\,m^{-2}\,K^{-4}}$ is the Stefan–Boltzmann constant. Emissivities of water and rock are close to 1, and temperatures in Eq. (51) are in Kelvin. Finally, the dry perimeter boundary condition is

$$k_\mathrm{r}\frac{\partial T_\mathrm{r,d}}{\partial y}\bigg|_{y=\text{ conduit wall}} = h_\mathrm{rad}(T_\mathrm{s,d} - T_\mathrm{w}), \tag{52}$$

where $T_\mathrm{r,d}$ is the temperature of the dry rock. As before, the wet perimeter boundary condition is given by Eq. (8), where $T_\mathrm{r} = T_\mathrm{r,w}$ (wet rock temperature), $T_\mathrm{s} = T_\mathrm{s,w}$ (wet conduit wall surface temperature), and r becomes y. We ~~ran~~ run three sets of simulations with different choices of recharge duration, $\mathcal{R}_\mathrm{D}$, with values equal to 1.67 h, 16.7 h, or 6.9 days. For each set, simulations

~~were~~ are run in planar coordinates with conduits that ~~were~~ are full, mostly full, half full, and mostly empty. A_w ~~was~~ is held constant for all open channel simulations to see how F and τ vary as a function of A_d. All simulations ~~were~~ are run with $D_\mathrm{H} = 1$ m to further facilitate comparisons. Because $\Theta \approx 22$ for all of these planar ~~simlations~~simulations, they accurately model heat exchange in cylindrical or planar conduits and permit simpler planar simulations (Covington et al., 2011). However, we also ~~ran~~ run a simulation with a full conduit in cylindrical coordinates for comparison to planar simulations for each set.

For the range of $A_\mathrm{d}/A_\mathrm{w}$ ratios and $\mathcal{R}_\mathrm{D}$ values considered, there is little difference in the transmission and retardation for each set of simulations with a given recharge duration (Table 4). In general, channels with a free surface undergo slightly more damping than channels that are completely full because there is more rock where heat may be exchanged in the open channel simulations. For the two sets of simulations with longer recharge durations, full planar simulations produce the least retardation, and conduits that are mostly full produce the most retardation.

7.3.4 Thermal recharge shape

Our numerical analysis thus far considers a Gaussian thermal recharge function. This is a rough approximation of the typical shape of thermographs found in natural systems, but natural pulses can display a variety of shapes. To explore the influence of shape on damping and retardation, we run simulations with a variety of other functions that are sometimes used to approximate natural pulses. Table 5 provides thermal transmission factors and retardation values for two sets of equivalent simulations in cylindrical coordinates. Each set includes a Gaussian function, two types of sine function segments, and a triangular function. Shapes of the recharge thermographs used are shown in Fig. 5. One of the sine-shaped peaks is composed of one period of a sine function from one trough to the next ($\mathrm{sine_O}$) and the other one as half a period between two consecutive zeros of the sine ($\mathrm{sine_H}$). $\mathcal{R}_\mathrm{D}$ for Gaussian functions is 6000 s and 60 000 s, respectively. Sine and triangular functions ~~were~~ are defined such that the total area under each curve was equal to the respective areas for the Gaussian functions. In both cases, the $\mathrm{sine_H}$ curve is the least damped and the triangular thermal recharge is the most damped, although the difference in F between the different recharge functions is small. For the shorter thermal pulse, the Gaussian pulse peaks first, and the triangle, sine_O, and sine_H peaks occur approximately ~~,~~ 4, 4, and 9 % later, respectively, than the Gaussian thermal pulse. For the longer thermal pulse, the triangle pulse peaks approximately 30 % earlier than the Gaussian peak, and the sine_O and sine_H peaks occur approximately 9 and 17 % later, respectively, than the Gaussian peak. There is less damping and more retardation for thermographs that have a wider peak/trough near the peak/trough, except for the triangle pulse with a $\mathcal{R}_\text{D} = 6000\,\text{s}$. However, the triangle pulse is not continuously differentiable, and numerical dispersion likely plays a role.

8 An example field ~~study~~ experiment to test components of the theory

Luhmann et al. (2012) conducted a ~~field-tracer~~ multitracer experiment at Freiheit Spring in southeastern Minnesota by filling a pool next to a sinkhole, heating the pool water, adding tracers, dumping the pool water into the sinkhole, and then monitoring spring breakthrough curves of discharge, temperature, chloride, uranine, delta deuterium, and suspended sediment. The ~~flow path~~straight-line, horizontal and vertical distances from the sinkhole to the spring are 95 m and 19 m, respectively. 54 % of the pool's thermal energy was recovered over the first two hours of the trace, which was lower than either the dye (66 %) or salt recoveries (78 %) over the same time period (Luhmann et al., 2012) . The dye recovery was lower than the salt recovery because of degradation, and the lower heat recovery occurred because of the damping of the thermal signal, where some of the heat was transferred into the rock surrounding the flow path. However, the heat from the heated rock was later transferred to subsequent water that flowed along the flow path, since water temperature at the spring remained higher than its background after experiment water no longer reached the spring. The flow path's D_H was estimated by reproducing the damped, retarded thermal signal from the trace with heat transport simulations. A much larger diameter was estimated by summing discharge between hydraulic and chemical responses, dividing by flow path distance, and assuming a circular conduit, but the estimate using the thermal pulse was in much better agreement with field observations.

We conducted a similar ~~study~~ experiment at the same site three days later. The pool was filled with approximately 12 600 L of water for the later study. The pool water was heated to 21.5°C, and 33.02 kg of NaCl were added. Discharge, temperature, electrical conductivity, and suspended sediment data were collected at the spring as the pool water was emptied into the sinkhole. This time, however, the pool was released as two separate pulses. Breakthrough curves are shown in Fig. 6, and all data but suspended sediment time series are provided in Luhmann (2011). Approximately the first half of the 12 600 L of water was released beginning at 16:27 LT on 2 September 2010, and the rest of the pool was emptied into the sinkhole beginning at 16:52 LT.

In general, spring breakthrough curves during this double pulse tracer test displayed similar responses to the single pour tracer experiment three days earlier (see Luhmann et al., 2012 for more discussion about the breakthrough curves from the earlier experiment). Discharge at Freiheit Spring increased shortly after each half of the pool was emptied into the sinkhole, suggesting full pipe flow conditions. Furthermore, the initial changes and peaks in suspended sediment occurred before the initial changes and peaks in conductivity. Finally, initial changes and peaks in temperature occurred later than the initial changes and peaks in conductivity because of temperature's non-conservative behavior.

Because these two field-scale experiments were conducted at the same site three days apart, all parameters that control F and τ except $\mathcal{R}_\mathrm{D}$ remained nearly constant. There was some rainfall between the two experiments which caused more background variability in spring parameters before the second study, but hydrodynamic conditions were very similar. Background spring discharges before the first and second traces were 26.7 and 26.8 $\mathrm{L\,s^{-1}}$, respectively. Additionally, it took 1082 s (Luhmann et al., 2012), 1066, and 1103 s between the pool dump (or partial pool dump) and each respective conductivity/chloride increase at the spring for the first trace, the first pulse of the second trace, and the second pulse of the second trace, respectively. Thus, flow-through time was similar for all three pours, and there was little to no variability in D_H, L, and V between the two experiments. However, $\mathcal{R}_\mathrm{D}$ was significantly changed from pour one during the first trace (Luhmann et al., 2012) to pours one and two during the second trace.

We did not collect any robust data at the sinkhole during the pours to provide quantitative $\mathcal{R}_\mathrm{D}$ information. However, the time span from the initial increase to the peak in electrical conductivity/chloride at the spring provides a proxy for $\mathcal{R}_\mathrm{D}$ during each pour. This took 625 s during the 30 August 2010 experiment ~~(Luhmann et al., 2012)~~ (Luhmann et al., 2012) and 502 and 464 s for the first and second pulses, respectively, of the 2 September 2010 experiment. Because τ is proportional to $\mathcal{R}_\mathrm{D}^{0.5}$, the thermal retardation in planar coordinates of the first or second pulse of the second experiment, ~~τ_Ex2~~ $\tau_\mathrm{pl,Ex2}$, is given by:

$$\tau_{\mathrm{Ex2}\,\mathrm{pl,Ex2}} = \tau_{\mathrm{Ex1}\,\mathrm{pl,Ex1}} \frac{\sqrt{\mathcal{R}_\mathrm{D,Ex2}}}{\sqrt{\mathcal{R}_\mathrm{D,Ex1}}} \tag{53}$$

where ~~τ_Ex1~~ $\tau_\mathrm{pl,Ex1}$ is the thermal retardation in planar coordinates from the first experiment and $\mathcal{R}_\mathrm{D,Ex1}$ and $\mathcal{R}_\mathrm{D,Ex2}$ are the recharge durations during single and double pulse experiments, respectively. With ~~τ_Ex1~~ $\tau_\mathrm{pl,Ex1}$ equal to 248 s (Luhmann et al., 2012), the predicted ~~τ_Ex2~~ $\tau_\mathrm{pl,Ex2}$ for the first and second pulses of the second experiment would be 222 s and 214 s, respectively. In reality, ~~τ_Ex2~~ $\tau_\mathrm{pl,Ex2}$ was 224 s and 218 s for the first and second pulses of the double pulse experiment, respectively, providing field evidence that $\tau \propto \mathcal{R}_\mathrm{D}^{0.5}$.

Samples were not analyzed for chloride during the double pulse tracer test. Thus, our uncertainty in calculating ~~F~~ the transmission factor from either pulse of the double pulse tracer test is larger than our uncertainty from the single pulse tracer test. ~~Therefore, we do not perform a similar calculation with F for the double pulse tracer study.~~ Furthermore, spring water temperature ~~was~~ and electrical conductivity were less stable before the double pulse study ~~, and damping of thermal peaks is less useful when there is more thermal variability in the time preceding the recharge period of interest. For example, during the double pulse study at Freiheit Spring, the second pulse produced~~ because of a recharge event that produced a minimum in conductivity and a maximum in temperature less than one day before the beginning of the experiment. Despite these uncertainties, a similar analysis can be performed with transmission using Eq. (36) as was done with retardation. The transmission factor in planar coordinates of the first or second pulse of the second experiment, $F_{\mathrm{pl,Ex2}}$, is given by:

$$F_{\mathrm{pl,Ex2}} = \exp\left(\frac{\ln F_{\mathrm{pl,Ex1}}\sqrt{\mathcal{R}_{\mathrm{D,Ex1}}}}{\sqrt{\mathcal{R}_{\mathrm{D,Ex2}}}}\right). \tag{54}$$

where $F_{\mathrm{pl,Ex1}}$ is the transmission factor in planar coordinates from the first experiment. With $F_{\mathrm{pl,Ex1}}$ equal to 39 % (Luhmann et al., 2012) , the predicted $F_{\mathrm{pl,Ex2}}$ for the first and second pulses of the second experiment would be 35 % and 33 %, respectively. By defining background temperature for each peak as the water temperature before each respective increase in temperature that led to each peak, $F_{\mathrm{pl,Ex2}}$ was 36 % and 34 % for the first and second pulses of the double pulse experiment, respectively. The heat recovery during the first two hours of the double pulse multitracer experiment (58 %) was higher than the heat recovery over the first two hours of the single pulse injection (54 %) because of the elevated rock temperatures from earlier water-rock heat exchange. This effect is ultimately responsible for the second pulse producing a higher temperature peak than the first pulse during the double pulse study, even though the second pulse produced a lower conductivity peak with a shorter $\mathcal{R}_{\mathrm{D}}$ (Fig. 6). The heated rock from the first pulse facilitated the propagation of a higher temperature peak during the second pulse. Thus, while the peak temperature from a later pulse is still useful, deriving flow path information from the peak temperature of a later pulse is more complicated than doing so using peak data from an initial pulse that follows a relatively stable background.

The best simulated fit of the temperature breakthrough curve from the single pulse tracer study ~~(Luhmann et al., 2012)~~ occurred with a $D_{\mathrm{H}} = 7\,\mathrm{cm}$ using a heat transport simulation in planar coordinates~~. The~~ (Luhmann et al., 2012) . The average flow-through time between the sinkhole and the spring from the initial increase in discharge to the initial increase in electrical/chloride at the spring was 1,075 s. Given the $\mathcal{R}_{\mathrm{D}}$ noted above and the values of rock and water physical properties provided in Table 1, then the best D_{H} estimate is 8 cm using τ data from this earlier study and Eq. (38). Similarly, the best D_{H} estimate is 5 cm using F data from this experiment and Eq. (36).

After these multitracer experiments were conducted, a caver used a trackhoe to excavate the sinkhole used for all injections and an abandoned steephead just southwest of Freiheit

Spring. Excavation of the sinkhole revealed a relatively flat, weathered bedrock surface with a vertical solution conduit about 20 cm in diameter developed down a vertical joint. The steephead indicates the location of a former spring, which was present long enough for headward erosion to develop the surface feature. The steephead excavation uncovered an underground stream flowing across the back of the steephead toward Freiheit Spring. Although a visual dye trace documented that the steephead flow did emerge at Freiheit Spring, we do not know for sure if water from the multitracer experiments passed through the steephead feature while flowing from the sinkhole to the spring. However, excavation at the steephead revealed a solutionally enlarged bedding plane parting with a height on the order of cms, in agreement with observations at the spring. For a very wide flow channel, $D_{\mathrm{H}} = 2h$, where h is the height of the conduit. Conduit height estimates using either the damping and retardation relationships or the numerical simulations range from 2.5-4 cm, in agreement with field observations.

9 Discussion

9.1 Information content of thermal damping and retardation

Variations in water quantity and quality at karst springs are often used to obtain information about the internal properties of a karst aquifer (e.g., Ashton, 1966; Atkinson, 1977b; Sauter, 1992; Ryan and Meiman, 1996; Birk et al., 2004, 2014; Luhmann et al., 2011; Luhmann et al., 2012; Covington et al., 2012). Specifically, Luhmann et al. (2012) showed that combining breakthrough curves of temperature and conservative tracers allows one to constrain values of flow path diameter. This was acheived by adjusting conduit parameters within a numerical transport simulation to obtain best fitting curves for tracer breakthrough. Here, we illustrate an alternative approach that employs the analytical solution for a sinusoidal recharge temperature. This solution provides a good approximation to the damping and retardation of Gaussian temperature pulses simulated over a wide range of conduit properties and recharge conditions. A single fitting parameter, C_{time}, was used to convert between the time scale of the sinusoidal pulse and the time scale of the Gaussian pulse. The primary advantage of this approach is that it is much easier to estimate a hydraulic diameter from analytical equations that relate to damping or retardation than it is to use a numerical model to try to find the best fitting breakthrough curve. Using the technique presented here, one can extract much of the information available in the breakthrough curve using one of these two numbers, damping or retardation.

The analytical solution provides ~~explict~~ explicit relationships for both the transmission (Eq. 36) and retardation (Eq. 38) of a thermal peak as a function of conduit properties (L and D_{H}), flow velocity, V, recharge duration, $\mathcal{R}_{\mathrm{D}}$, and quantities that are related to the thermal properties of water and rock (Ψ and α_{r}). The thermal properties of water and rock are relatively constant within a given aquifer, and even do not vary that substantially among near-surface karst aquifers. While an estimate of these parameters is needed to relate damping and retardation to conduit properties, once an estimate is made we typically can treat these as constants for a given site. The conduit length and velocity only occur in Eqs. (36) and (38) as a ratio, L/V, which is equal to the flow-through time, t_{ft}. Therefore, we can reduce these two parameters to a single parameter that is also physically meaningful and more easily measured in the field. This leaves three variables, t_{ft}, $\mathcal{R}_{\mathrm{D}}$, and D_{H}, that relate to the damping and retardation via two equations. Therefore, if both damping and retardation are measured at a field site, then we have two equations and three unknowns. One might expect that only one of these three unknowns would need to be constrained by additional field data, and then the other two could be calculated from the relations. However, the relations for damping and retardation are not entirely linearly independent, and therefore contain some duplicate information.

A Maclaurin Series expansion of the exponential in Eq. (36) shows that for low to moderate amounts of damping the transmission factor, F, scales roughly as

$$(1-F) \propto \frac{t_{\mathrm{ft}}}{D_{\mathrm{H}}\mathcal{R}_{\mathrm{D}}^{0.5}}. \tag{55}$$

Regardless of the extent of damping, the retardation scales as

$$\tau \propto \frac{t_{\mathrm{ft}}\mathcal{R}_{\mathrm{D}}^{0.5}}{D_{\mathrm{H}}}. \tag{56}$$

Since t_{ft} and D_{H} enter both relations in the same combination, one of these two variables must be constrained from data in order to solve for the other variables. This conclusion only holds for the low damping regime, but this is also the regime in which damping or retardation could feasibly be measured in the field.

These considerations about the independence of the damping and retardation equations are largely theoretical. In real world cases, both t_{ft} and $\mathcal{R}_{\mathrm{D}}$ are relatively easy to measure, and it is more likely that both of these will be measured and then used to make separate estimates of D_{H} using both the damping and retardation equations. If these duplicate estimates are substantially different from each other, then it would suggest that some assumptions of the model are being broken or that one or more of the measurements was in error.

Thermal damping and retardation are not affected by the recharge amplitude ($\mathcal{R}_{\mathrm{A}}$) or the thermal conductivity (k_{w}) or dynamic viscosity of water (μ_{w}). However, it may be impossible to determine F and τ information if $\mathcal{R}_{\mathrm{A}}$ is small. Thus, recharge temperatures that are further from background temperatures make it more practical to use water temperature as a tracer to potentially provide flow path information.

9.2 Limitations of the model

A fairly large number of simplifying assumptions separate the analytical solution presented above from a natural karst conduit. Therefore, it is worth considering the likely effects of these assumptions, and the extent to which the solution will fail in different settings. Among the assumptions behind the analytical solution are: (1) a sinusoidal recharge temperature, (2) a single conduit diameter, (3) no longitudinal dispersion, (4) constant discharge, and (5) rock and water thermal properties that are constant throughout the system.

While seasonal temperature variations might be well represented by a sinusoidal solution, most temperature variations at karst springs come in the form of short peaks due to recharge events. However, the numerical simulations presented above demonstrate that, with the help of a fitting parameter, the sinusoidal solution for damping and retardation can be applied to a variety of single-peak functions, including Gaussians, a triangle pulse, and sine peaks. This may not be the case for multipeak functions, particularly if the peaks are more closely spaced than those of the sinusoidal function. In that case, earlier peaks will likely influence the behavior of later peaks.

The analytical solution allows estimation of a single conduit diameter, whereas karst conduits can display a substantial variation in diameter along their length. Therefore a key question is how this estimated diameter is related to the physical conduit properties. The estimated diameter is the diameter of an equivalent conduit that produces the same thermal damping and retardation. It is possible to derive more than one equivalent model depending upon the constraints and assumptions applied. However, for a seemingly reasonable set of constraints the effective diameter is the flow-through time weighted harmonic mean of the hydraulic diameter of the real conduit. To derive this equivalent model, it was assumed that the thermograph time scale does not substantially change as it passes through the system. For the two example simulation sets, the equivalent diameter, so defined, produces the same transmission and retardation as a multi-segment conduit with different diameters (Sect. 7.3.1). This provides some verification that the approach is reasonable, though the approximation is likely to break down for cases where the flow-through time is much longer than the pulse duration. However, this is also the limit in which pulses will be substantially damped and difficult or impossible to observe.

Rather than consisting of a single flow path, natural karst conduits typically contain a network of flow paths of various sizes. Branchwork patterns are quite common, but a variety of network topologies are possible. Physical interpretation of thermal damping and retardation is most straightforward when the system is dominated by a single flow path, such as a sink-rise system. In this case, estimates of conduit diameter apply to the primary conduit. However, ~~thermal tracing experiments between injection points~~ a thermal tracing experiment between an injection point and a spring, as conducted by Luhmann et al. (2012), may also allow characterization of conduit ~~diameters~~ diameter along the flow path between those two points. It is less clear how to interpret natural temperature pulses at a spring fed by a branchwork system, since water arriving at the spring will have flowed via a large number of different paths of different lengths and diameters. In such cases, network properties are likely to play a significant role, and a better understanding of heat transport within networks is required.

The analytical solution also assumes that longitudinal dispersion can be neglected. While karst conduits tend to have high Peclet numbers, and therefore be advection-dominated, dispersion is certain to play a role for increasingly short duration pulses. Therefore care is needed when applying this solution to short injection pulses, particularly if they propagate a substantial distance. However, the tracer pulses described in Sect. 8 are relatively short, and still display the scaling predicted by the theory. In that case, the flow path was also short, which may minimize the influence of dispersion. In addition to longitudinal dispersion, immobile fluid regions such as pools and eddys can substantially influence tracer behavior (Field and Pinsky, 2000). Again, such effects are likely to be largest for short-duration pulses.

The solution assumes constant discharge in time and with distance along the conduit. In Sect. 7.3.2, we use simulations to explore the effect of varying discharge in time. We find that discharge variability has a relatively modest effect on damping and retardation, and that the direction of the effect is dependent upon the relative magnitude of the flow-through time and recharge duration. ~~Addition of water along the conduit may also have a substantial effect. If the main conduit flow is diluted by water recharged through more diffuse (e. g. , matrix or fracture)flow paths, then that water will cause additional damping of the pulse. A gradual addition of matrix water can also influence the retardation, albeit less substantially.~~ Our choice of velocity variation is only one of many approximations to natural flow variations, and variability in nature is certainly more complex. While it is difficult to generalize when the constant velocity assumption introduces large errors, the analytical solutions can be used to provide some constraints on the effect of the constant velocity simplification. For example, consider flow through a karst conduit where discharge is not constant, but zero for the first half of the flow-through time and twice the average discharge value for the second half. By comparing to an equivalent conduit with constant discharge and the same water volume in the pulse, the velocity and recharge duration in the non-constant discharge conduit would be $2V$ and $\mathcal{R}_{\mathrm{D}}/2$, respectively. If we determine F, then the term in parenthesis in Eq. (36) would be $1/\sqrt{2}$ times what it would be with constant discharge. Similarly, given τ, the term on the right side of Eq. (38) would be $0.5/\sqrt{2}$ times what it would be with constant discharge. Therefore, the ratio $L/(VD_{\mathrm{H}})$ in Eqs. (36) and (38) would be $1/\sqrt{2}$ and $0.5/\sqrt{2}$ times, respectively, of the actual value. Given an estimate of flow-through time (L/V), the calculated conduit length would be 1/2 of the true value, and the hydraulic diameter would be underestimated and overestimated by a factor of $\sqrt{2}$ using either the damping or retardation relationships, respectively. Still, it is likely that discharge variability will introduce too much uncertainty and limit the applicability of the damping and retardation analytical solutions in some field scenarios. However, the multitracer studies at Freiheit Spring suggest that the damping and retardation relationships may provide useful results even when there are variations in velocity.

The analytical solution does not account for hydraulic exchange between the conduit and the matrix (or fractures or other conduits). Flow from the conduit to the matrix will affect heat flux in the matrix, and the changed heat flux in the matrix would only have a small, indirect influence on the water temperature in the conduit. In contrast, flow from the matrix to the conduit would have a direct and significant effect on the water temperature in the conduit. However, in this case, the thermal modification of the water is due to mixing of two water sources with different temperatures or dilution of the input rather than damping that occurs due to heat exchange between water and rock. The influence of dilution on the transmission factor can be approximated using a simple mixing model, where the effects of dilution and heat exchange are assumed to be separable. The applicable bounds of this approximation are discussed for linear processes in 10001000[Eq. 31]covington12, who conclude that the separated treatment of dilution and damping is a good approximation for cases where the signal is not severely damped. The same conclusion applies when heat exchange can be treated as approximately linear, which is also in the regime where damping is not too severe. However, more work is needed to quantify more precisely the conditions under which this separable model breaks down. To account for dilution with a simple mixing model, the peak input temperature is first reduced by the fraction that would be calculated from simple mixing. Then the heat transport model is applied. For example, during the multitracer study in Luhmann et al. (2012) , the injected pool water temperature (24.1°C) produced a peak water temperature at Freiheit Spring of 11.45°C, above the spring background temperature of 9.08°C. Without accounting for dilution/mixing, transmission is incorrectly calculated as 16 %. However, chloride concentration from the trace was used to determine the extent of mixing, indicating that the 24.1°C pool water temperature was reduced to a maximum of 15.19°C along the flow path due to mixing with water from other sources. By accounting for this mixing, transmission is actually 39 %. Flow from the matrix to the conduit would likely have a small effect on retardation in the conduit that will ultimately depend on the spatial distribution of the matrix input. Further simulations and field experiments could better quantify the effects of dilution~~and~~ /mixing.

Finally, the thermal properties of rock and water are assumed to be constant throughout the aquifer. While the thermal properties of carbonate rocks within karst aquifers can be somewhat variable (Beardsmore and Cull, 2001), uncertainty can be reduced if measured thermal properties for specific formations of interest are available. However, there are still some potential limitations. In particular, many karst conduits contain a substantial layer of sediments on the floor. The heat transfer properties of such sediments are likely to be more variable than that of the solid rock at the field site of interest, and in some cases hyporheic exchange is likely to play an important role.

9.3 Considerations for field studies

Determination of the damping and retardation of a thermal peak requires high resolution data for both temperature and a conservative tracer in order to capture sharp features in the data. In some cases, data output intervals may need to be on the order of seconds to provide sufficient constraints on the timing and magnitude of thermal peaks/troughs. Due to memory or power limitations, data are not often collected at such a high frequency. Consequently, deploying loggers with the capacity to modify data output intervals based on real-time monitoring, or with the capability to transfer data remotely in real time, may be particularly useful.

Monitoring installations in karst frequently have equipment to record water level, electrical conductivity, and temperature. In general, water level data has little use in determining retardation, since initial hydrograph perturbations often record arrival of pre-event water. Even in the case of open channel conduits, the discharge pulse, which travels as a kinematic wave, will arrive before the event water. In contrast, spring electrical conductivity perturbations can record event water arrival (e.g., Raeisi et al., 2007), and electrical conductivity interacts more slowly with the rock surrounding a conduit than temperature (Birk et al., 2006; Covington et al., 2012).

Thus, in many cases, retardation may be estimated as the time difference between the electrical conductivity and temperature peaks or troughs.

Determining the damping of a thermal peak requires an estimate of recharge temperature, in addition to a thermograph at the spring. In some cases, recharge temperature can be monitored at an upstream monitoring location. If this is not possible, recharge temperature may also be approximated in some special cases, such as during a snowmelt event. Dilution can ~~also have a strong effect on damping~~significantly modify recharge temperatures, and therefore an estimate of dilution is needed for damping calculations, for example by measuring flow at the recharge and discharge points.

While it can be relatively easy to determine thermal retardation using electrical conductivity and temperature data at some monitoring location of interest, interpretation of thermal damping and retardation is most easily accomplished in systems that contain a sinking surface stream. The values of thermal damping and retardation can be estimated during periods of relatively constant discharge between precipitation events. While flow-through time remains relatively constant during these periods, oscillations in surface stream recharge temperature will cause diurnal thermal oscillations at a downstream monitoring location, so long as heat exchange along the conduit is sufficiently ineffective (Luhmann et al., 2011). Measuring discharge at both upstream and downstream monitoring locations allows an estimate of the degree of dilution that occurs along the flow path to facilitate determination of F and constrain potential uncertainty in the measurement of τ and F. Injection of a conservative tracer permits estimates of flow-through time, and thus facilitates calculation of τ when used in conjunction with the travel time of diurnal thermal peaks or troughs from the upstream to the downstream monitoring locations. Measurements of damping and retardation in a sink-rise system are more difficult to obtain during natural recharge events, since temperature and recharge rates may vary independently, and flow-through time will also vary throughout the event. However, simultaneous monitoring of conductivity and temperature at the recharge and discharge points, particularly if combined with recharge and discharge hydrographs, may still enable measurement of damping and retardation in many settings.

In addition to sink-rise systems, interpretation of damping and retardation may be relatively straightforward during tracer studies with a known recharge input. In this case, the more heavily the system is perturbed, the easier it will be to interpret the results. In general, the ratio of conduit length to the thermal length scale provided in Eq. (23) can be used to estimate conditions where it would be possible to perform a thermal tracer study and observe water temperature perturbations at the outlet. This ratio is the thermal process number (Covington et al., 2012) , $\Lambda_{\mathrm{T,sin}}$, and is given by

$$\Lambda_{\mathrm{T,sin}} = \frac{L}{\lambda_{\mathrm{T,sin}}} = \frac{4L}{V\Psi D_{\mathrm{H}}}\sqrt{\frac{\pi\alpha_{\mathrm{r}}}{2C_{\mathrm{time}}\mathcal{R}_{\mathrm{D}}}}, \tag{57}$$

where we use the same relation for ω as in Eq. (36). If $\Lambda_{\mathrm{T,sin}} \lesssim 1$, then a thermal trace should change water temperature at the outlet, so long as estimates of variables in Eq. (57) are appropriate. If $\Lambda_{\mathrm{T,sin}} \gg 1$, then thermal variations will be completely damped, which still permits estimates of a threshold or maximum conduit diameter (Birk et al., 2014) . Regardless of the outcome, thermal tracer studies will generally provide useful results, while either confirming predictions or exposing errors in parameter estimates.

If recharge can be monitored, then $\mathcal{R}_{\mathrm{D}}$ is given by the full width at half maximum of the recharge thermograph (Eq. 33). The actual shape of the pulse will ultimately be a source of uncertainty. When recharge cannot be monitored, a related time scale to the $\mathcal{R}_{\mathrm{D}}$ is given by the time from the initial change to the peak/trough in a chemograph during a recharge event, as we did in Sect. 8. If necessary, the time from the initial change to the peak/trough in a thermograph may be used, although the thermograph will not be as accurate since the pulse is modified.

Both thermal damping and retardation data can potentially be used to estimate the hydraulic diameter of a karst conduit. However, measurement of retardation, rather than damping, has inherent advantages. There is better agreement in τ between analytical solutions and numerical simulations than there is with F. This suggests that estimates of D_{H} may have less uncertainty when using τ values. Furthermore, it is easier to determine τ in the field than F, since estimates of τ only require temperature and electrical conductivity data at the monitoring location of interest, whereas estimates of F also require information about recharge into the system. Finally, damping ~~is more severely impacted by any~~ requires an accounting of dilute inflow occuring along the flow path.

10 Conclusions

As water flows through an aquifer, heat exchange occurs between water and rock if they are in thermal disequilibrium. When thermal equilibrium is not attained, the water-rock interaction produces a damped thermal signal in the water that is retarded behind the actual groundwater velocity. Our analytical derivations and numerical simulations demonstrate that the damping and retardation of thermal peaks in conduits or fractures depend on the flow path's hydraulic diameter (D_H), flow-through time (L/V), and the timescale of the temperature variation ($\mathcal{R}_\mathrm{D}$). Damping and retardation are also dependent on rock thermal conductivity ~~,~~ (k_r), rock specific heat ~~,~~ ($c_\mathrm{p,r}$), rock density ~~,~~ (ρ_r), water specific heat ~~,~~ ($c_{p,\mathrm{w}}$), and water density ~~,~~ (ρ_w). However, these parameters vary relatively little within shallow aquifers. Because of this, the relationships for damping and retardation developed here may be used to estimate the hydraulic diameter of a flow path given estimates of the flow-through time and the timescale of temperature variations. Our tracer studies at Freiheit Spring provide some evidence for the applicability of these relationships. Additional field work is needed to test the usefulness of these relationships when working with more complex flow paths found in nature.

Simulations with variable D_H or V, open channels, and sine- or triangular-shaped thermograph shapes produce some variability in F and τ when compared to simulations with constant D_H or V, full pipe flow, and Gaussian-shaped thermographs. However, variability is generally small, and uncertainty from these conditions should not prevent estimates of D_H using F and τ. In general, estimates of D_H from natural conduits with variable D_H represent a flow-through time weighted harmonic mean of D_H. The effect of variable V on F and τ relationships is more complex, and additional work is necessary to further understand the effect of the shape and timing of different velocity functions on spring thermographs. Finally, the difference in F and τ between conduits with or without free water surfaces depends on the time scale of temperature variation, but open channels will produce somewhat more damping and retardation than conduits that are water-filled.

Luhmann et al. (2012) conducted a field tracer experiment that involved temperature, conductivity/chloride, and other parameters. They were able to estimate a flow path's D_{H} using known recharge data, high resolution output data, and heat transport simulations which reproduced the damped, retarded thermal signal that resulted from the trace. The dependence of F and τ on D_{H} derived here enables a new technique. Specifically, one may estimate the conduit diameter using observations of only the damping and retardation of thermal pulses from natural recharge events or tracer experiments. There is likely more error in D_{H} estimates using this new technique. However, it allows extraction of much of the information carried by the thermal pulses with the ease of employing an analytical solution.

The Supplement related to this article is available online at doi:10.5194/hessd-0-1-2014-supplement.

Acknowledgements. A. J. Luhmann was supported by a Doctoral Dissertation Fellowship from the University of Minnesota Graduate School. J. M. Myre was supported by the National Science Foundation (NSF) through an Earth Sciences Postdoctoral Fellowship (EAR-1249895). M. O. Saar acknowledges the NSF under Grant EAR-0941666. Any opinions, findings, and conclusions or recommendations expressed in this material are those of the authors and do not necessarily reflect the views of the NSF. M. O. Saar also thanks the ETH-Zürich for its endowment support by the Werner Siemens Foundation of the Geothermal Energy and Geofluids Group as well as the George and Orpha Gibson Endowment for its support of the Hydrogeology and Geofluids Group in the Department of Earth Sciences at the University of Minnesota. Funding for the pool trace study at Freiheit Spring was provided by the Minnesota Environment and Natural Resources Trust Fund as recommended by the Legislative-Citizen Commission on Minnesota Resources (LCCMR). We thank Susan, Aaron, and Matt Kolling for access to their property at Freiheit Spring, and Greg Brick, Su Yi Chai, Dwight Luhmann, and Peter Putzier for assistance with the pool trace study.

References

Ashton, K.: The analysis of flow data from karst drainage systems, The Transactions of the Cave Research Group, 7, 161–203, 1966.

Atkinson, T. C.: Carbon dioxide in the atmosphere of the unsaturated zone: An important control of groundwater hardness in limestones, J. Hydrol., 35, 111–123, 1977a.

Atkinson, T. C.: Diffuse flow and conduit flow in limestone terrain in the Mendip Hills, Somerset (Great Britain), J. Hydrol., 35, 93–110, 1977b.

Beardsmore, G. R. and Cull, J. P.: Crustal Heat Flow: A Guide to Measurement and Modelling, Cambridge University Press, Cambridge, UK, 2001.

Benderitter, Y., Roy, B., and Tabbagh, A.: Flow characterization through heat transfer evidence in a carbonate fractured medium: first approach, Water Resour. Res., 29, 3741–3747, 1993.

Birk, S., Liedl, R., and Sauter, M.: Identification of localised recharge and conduit flow by combined analysis of hydraulic and physico-chemical spring responses (Urenbrunnen, SW-Germany), J. Hydrol., 286, 179–193, 2004.

Birk, S., Liedl, R., and Sauter, M.: Karst spring responses examined by process-based modeling, Ground Water, 44, 832–836, 2006.

Birk, S., Wagner, T., and Mayaud, C.: Threshold behavior of karst aquifers: the example of the Lurbach karst system (Austria), Environ. Earth Sci., doi:10.1007/s12665-014-3122-z, in press, 2014.

Boussinesq, J.: Sur un mode simple d'écoulement des nappes d'eau d'infiltration à lit horizontal, avec rebord vertical tout autour lorsqu'une partie de ce rebord est enlevée depuis la surface jusqu'au fond, CR Acad. Sci., 137, 5–11, 1903.

Boussinesq, J.: Recherches théoretiques sur l'écoulement des nappes d'eau infiltrées dans le sol et sur le débit des sources, J. Math. Pure. Appl., 10, 5–78, 1904.

Bundschuh, J.: Temporal variations of spring water temperatures in relation to the extents of heat transport modes occurring in the karstified lower Gypsum-Keuper aquifer (Karnian, southern Germany), in: Proceedings of the 12th International Congress of Speleology, 6th Conference on Limestone Hydrology and Fissured Media, 10–17 August 1997, La Chaux de Fonds, Switzerland, vol. 2, 129–132, 1997.

Covington, M. D., Wicks, C. M., and Saar, M. O.: A dimensionless number describing the effects of recharge and geometry on discharge from simple karstic aquifers, Water Resour. Res., 45, W11410, doi:10.1029/2009WR008004, 2009.

Covington, M. D., Luhmann, A. J., Gabrovšek, F., Saar, M. O., and Wicks, C. M.: Mechanisms of heat exchange between water and rock in karst conduits, Water Resour. Res., 47, W10514, doi:10.1029/2011WR010683, 2011.

Covington, M. D., Luhmann, A. J., Wicks, C. M., and Saar, M. O.: Process length scales and longitudinal damping in karst conduits, J. Geophys. Res.-Earth, 117, F01025, doi:10.1029/2011JF002212, 2012.

Dewandel, B., Lachassagne, P., Bakalowicz, M., Weng, P., and Al-Malki, A.: Evaluation of aquifer thickness by analysing recession hydrographs. Application to the Oman ophiolite hard-rock aquifer, J. Hydrol., 274, 248–269, 2003.

Doucette, R. and Peterson, E. W.: Identifying water sources in a karst aquifer using thermal signatures, Environ. Earth Sci., doi:10.1007/s12665-014-3387-2, in press, 2014.

Field, M. S. and Nash, S. G.: Risk assessment methodology for karst aquifers: (1) Estimating karst conduit-flow parameters, Environ. Monit. Assess., 47, 1–21, 1997.

Field, M. S. and Pinsky, P. F.: A two-region nonequilibrium model for solute transport in solution conduits in karstic aquifers, J. Contam. Hydrol., 44, 329–351, 2000.

Ford, D. C. and Williams, P.: Karst Hydrogeology and Geomorphology, John Wiley & Sons, Chichester, England, 2007.

Gunn, J.: Analysis of groundwater pathways by high temporal resolution water temperature logging in the Castleton Karst, Derbyshire, England, in: Hydrogeological and Environmental Investigations in

Karst Systems, edited by: Andreo, B., Carrasco, F., Durán, J. J., Jiménez, P., and LaMoreaux, J. W., Springer, Berlin Heidelberg, 227–235, 2015.

Hall, F. R.: Base-flow recessions – a review, Water Resour. Res., 4, 973–983, 1968.

Hauns, M., Jeannin, P.-Y., and Atteia, O.: Dispersion, retardation and scale effect in tracer breakthrough curves in karst conduits, J. Hydrol., 241, 177–193, 2001.

Incropera, F. P., DeWitt, D. P., Bergman, T. L., and Lavine, A. S.: Fundamentals of Heat and Mass Transfer, 6th Edn., John Wiley & Sons, Hoboken, New Jersey, USA, 2007.

Jakucs, L.: Neue methoden der höhlenforschung in Ungarn und ihre ergebnisse, Die Höhle, 10, 88–98, 1959.

Jeannin, P.-Y. and Sauter, M.: Analysis of karst hydrodynamic behaviour using global approaches: A review, Bulletin d'Hydrogéologie, 16, 31–48, 1998.

Liedl, R. and Sauter, M.: Modelling of aquifer genesis and heat transport in karst systems, Bulletin d'Hydrogéologie, 16, 185–200, 1998.

Liedl, R., Renner, S., and Sauter, M.: Obtaining information about fracture geometry from heat flow data in karst systems, Bulletin d'Hydrogéologie, 16, 143–153, 1998.

Luhmann, A. J.: Water Temperature as a Tracer in Karst Aquifers, Ph.D. thesis, available at: http://purl.umn.edu/113204, University of Minnesota, Minneapolis, Minnesota, USA, 2011.

Luhmann, A. J., Covington, M. D., Peters, A. J., Alexander, S. C., Anger, C. T., Green, J. A., Runkel, A. C., and Alexander Jr., E. C.: Classification of thermal patterns at karst springs and cave streams, Ground Water, 49, 324–335, 2011.

Luhmann, A. J., Covington, M. D., Alexander, S. C., Chai, S. Y., Schwartz, B. F., Groten, J. T., and Alexander Jr., E. C.: Comparing conservative and nonconservative tracers in karst and using them to estimate flow path geometry, J. Hydrol., 448–449, 201–211, 2012.

Maillet, E. T.: Essais d'Hydraulique Souterraine & Fluviale, Hermann, Paris, 1905.

Markle, J. M. and Schincariol, R. A.: Thermal plume transport from sand and gravel pits – Potential thermal impacts on cool water streams, J. Hydrol., 338, 174–195, 2007.

Martin, J. B. and Dean, R. W.: Temperature as a natural tracer of short residence times for groundwater in karst aquifers, in: Karst Modeling, Special Publication 5, edited by: Palmer, A. N., Palmer, M. V., and Sasowsky, I. D., Karst Waters Institute, Charles Town, West Virginia, USA, 236–242, 1999.

Molson, J. W., Frind, E. O., and Palmer, C. D.: Thermal energy storage in an unconfined aquifer: 2. Model development, validation, and application, Water Resour. Res., 28, 2857–2867, 1992.

Molson, J. W., Pehme, P., Cherry, J., and Parker, B.: Numerical analysis of heat transport within fractured sedimentary rock: Implications for temperature probes, in: Proceedings: NGWA/U.S. EPA Frac-

tured Rock Conference: State of the Science and Measuring Success in Remediation, 24–26 September 2007, Portland, Maine, USA, 2007.
Newson, M. D.: A model of subterranean limestone erosion in the British Isles based on hydrology, T. I. Brit. Geogr., 54, 55–70, 1971.
O'Driscoll, M. A. and DeWalle, D. R.: Stream–air temperature relations to classify stream–ground water interactions in a karst setting, central Pennsylvania, USA, J. Hydrol., 329, 140–153, 2006.
Palmer, C. D., Blowes, D. W., Frind, E. O., and Molson, J. W.: Thermal energy storage in an unconfined aquifer: 1. Field injection experiment, Water Resour. Res., 28, 2845–2856, 1992.
Raeisi, E., Groves, C., and Meiman, J.: Effects of partial and full pipe flow on hydrochemographs of Logsdon River, Mammoth Cave Kentucky USA, J. Hydrol., 337, 1–10, 2007.
Renner, S.: Wärmetransport in Einzelklüften und Kluftaquiferen – Untersuchungen und Modellrechnungen am Beispiel eines Karstaquifers, Ph.D. thesis, Tübinger Geowissenschaftliche Arbeiten C30, University of Tübingen, Tübingen, Germany, 1996.
Ryan, M. and Meiman, J.: An examination of short-term variations in water quality at a karst spring in Kentucky, Ground Water, 34, 23–30, 1996.
Sauter, M.: Quantification and Forecasting of Regional Groundwater Flow and Transport in a Karst Aquifer (Gallusquelle, Malm, SW. Germany), Ph.D. thesis, Tübinger Geowissenschaftliche Arbeiten C13, University of Tübingen, Tübingen, Germany, 1992.
Screaton, E., Martin, J. B., Ginn, B., and Smith, L.: Conduit properties and karstification in the unconfined Floridan Aquifer, Ground Water, 42, 338–346, 2004.
Tallaksen, L. M.: A review of baseflow recession analysis, J. Hydrol., 165, 349–370, 1995.
Ternan, J. L.: Comments on the use of a calcium hardness variability index in the study of carbonate aquifers: With reference to the Central Pennines, England, J. Hydrol., 16, 317–321, 1972.
White, W. B.: Karst hydrology: Recent developments and open questions, Eng. Geol., 65, 85–105, 2002.
Worthington, S. R. H.: A comprehensive strategy for understanding flow in carbonate aquifers, in: Karst Modeling, Special Publication 5, edited by: Palmer, A. N., Palmer, M. V., and Sasowsky, I. D., Karst Waters Institute, Charles Town, West Virginia, USA, 30–37, 1999.
Worthington, S. R. H., Davies, G. J., and Quinlan, J. F.: Geochemistry of springs in temperate carbonate aquifers: Recharge type explains most of the variation, in: Annales Scientifiques de l'Université de Besançon, Geologie–Mémoire Hors Série, edited by: Chauve, P. and Zwahlen, F., Cinquième Colloque d'Hydrologie en Pays Calcaire et en Milieu Fissuré, 16–18 October 1992, Neuchâtel, Switzerland, 11, 341–347, 1992.

Worthington, S. R. H., Ford, D. C., and Beddows, P. A.: Porosity and permeability enhancement in unconfined carbonate aquifers as a result of dissolution, in: Speleogenesis: Evolution of Karst Aquifers, edited by: Klimchouk, A. V., Ford, D. C., Palmer, A. N., and Dreybrodt, W., National Speleological Society of America, Huntsville, Alabama, USA, 220–223, 2000.

Table 1. Default parameters used in simulations.

Parameter	Value	Units
D_{H}	1	m
L	1000	m
V	0.626	$\mathrm{m\,s^{-1}}$
$\mathcal{R}_{\mathrm{A}}$	10	$^{\circ}\mathrm{C}$
$\mathcal{R}_{\mathrm{D}}$	60 000	s
k_{r}	2.15	$\mathrm{W\,m^{-1}\,^{\circ}C^{-1}}$
$c_{\mathrm{p,r}}$	810	$\mathrm{J\,kg^{-1}\,^{\circ}C^{-1}}$
ρ_{r}	2320	$\mathrm{kg\,m^{-3}}$
k_{w}	0.58	$\mathrm{W\,m^{-1}\,^{\circ}C^{-1}}$
$c_{p,\mathrm{w}}$	4200	$\mathrm{J\,kg^{-1}\,^{\circ}C^{-1}}$
ρ_{w}	1000	$\mathrm{kg\,m^{-3}}$
μ_{w}	1.3×10^{-3}	$\mathrm{kg\,s^{-1}\,m^{-1}}$
D_{L}	0.01	$\mathrm{m^2\,s^{-1}}$
Pr	9.5	–

Table 2. Thermal transmission factors and retardation values of variable D_H and constant $D_\mathrm{H,e}$ simulations.

D_H or ~~$D_\mathrm{H,E}$~~ $D_\mathrm{H,e}$ (m)	L (m)	V ($\mathrm{m\,s^{-1}}$)	F (–)	τ (s)
1 and 1.2	2500 and 2500	0.144 and 0.1	0.42	2220
1.11	4959	0.117	0.42	2220
1 and 2	2500 and 2500	0.4 and 0.1	0.65	1040
1.67	4500	0.144	0.65	1050

Other parameters different from values in Table 1: $\mathcal{R}_\mathrm{D} = 6000\,\mathrm{s}$.

Table 3. Thermal transmission factors and retardation values of variable V and equivalent constant V simulations.

V ($\mathrm{m\,s^{-1}}$)	$\mathcal{R}_\mathrm{D}$ (s)	L/V (s)	$\mathcal{R}_\mathrm{D}$ to L/V ratio	F (–)	τ (s)
variable (but more time at V below average V)	600	49 680	$\ll 1$	0.10	1470
0.101	600	49 680	$\ll 1$	0.06	1360
variable (but more time at V below average V)	6000	46 806	< 1	0.43	3900
0.107	6000	46 806	< 1	0.34	2800
variable (but more time at V below average V)	33 000	32 356	~ 1	0.70	5400
0.155	33 000	32 356	~ 1	0.70	4500
variable (but more time at V above average V)	60 000	27 194	> 1	0.78	4700
0.184	60 000	27 194	> 1	0.79	5100
variable (but more time at V above average V)	600 000	25 020	$\gg 1$	0.91	14 600
0.200	600 000	25 020	$\gg 1$	0.91	15 400

Other parameters different from values in Table 1: $L = 5000\,\mathrm{m}$.

Table 4. Thermal transmission factors and retardation values of open channel simulations with different $A_\mathrm{d}/A_\mathrm{w}$ ratios.

Channel type	$\mathcal{R}_\mathrm{D}$ (s)	A_w (–)	A_d (–)	F (–)	τ (s)
Full	6000			0.80	540
Full – cylindrical	6000			0.79	530
Mostly full	6000	3	1.4	0.79	540
Half full	6000	3	3	0.79	540
Mostly empty	6000	3	11	0.79	540
Full	60 000			0.93	1800
Full – cylindrical	60 000			0.92	1830
Mostly full	60 000	3	1.4	0.92	1850
Half full	60 000	3	3	0.92	1830
Mostly empty	60 000	3	11	0.92	1810
Full	600 000			0.98	5800
Full – cylindrical	600 000			0.96	6100
Mostly full	600 000	3	1.4	0.97	6600
Half full	600 000	3	3	0.97	6400
Mostly empty	600 000	3	11	0.96	6100

Other parameters different from values in Table 1: $V = 0.1\ \mathrm{m\,s^{-1}}$.

Table 5. Thermal transmission factors and retardation values of different recharge shape simulations.

Thermograph shape	$\mathcal{R}_\mathrm{D}$ (s)	F (–)	τ (s)
$\mathrm{Sine_H}$	6000	0.34	3220
$\mathrm{Sine_O}$	6000	0.33	3090
Gaussian	6000	0.32	2960
Triangle	6000	0.31	3090
$\mathrm{Sine_H}$	60 000	0.66	10 900
$\mathrm{Sine_O}$	60 000	0.65	10 100
Gaussian	60 000	0.65	9300
Triangle	60 000	0.62	6500

Other parameters different from values in Table 1:
$L = 5000\,\mathrm{m}$ and $V = 0.1\ \mathrm{m\,s^{-1}}$.

Table 6. Notation.

A_d	$P_\mathrm{d}/W_\mathrm{fs}$ (unitless)
A_w	$P_\mathrm{w}/W_\mathrm{fs}$ (unitless)
$c_{p,\mathrm{r}}$	specific heat capacity of rock ($\mathrm{J\,kg^{-1}\,^\circ C^{-1}}$)
$c_{p,\mathrm{w}}$	specific heat capacity of water ($\mathrm{J\,kg^{-1}\,^\circ C^{-1}}$)
C_cyl	correction factor for damping in cylindrical coordinates (unitless)
C_time	time conversion constant (unitless)
D_H	conduit hydraulic diameter (m)
$D_\mathrm{H,avg}$	average conduit hydraulic diameter (m)
$D_\mathrm{H,e}$	effective conduit hydraulic diameter (m)
$D_{\mathrm{H},i}$	conduit hydraulic diameter of segment i (m)
D_L	longitudinal dispersivity ($\mathrm{m^2\,s^{-1}}$)
f	Darcy–Weisbach friction factor (unitless)
F	thermal transmission factor (unitless)
F_cyl	thermal transmission factor in cylindrical coordinates (unitless)
F_i	thermal transmission factor of segment i (unitless)
$F_\mathrm{pl,Ex1}$	thermal transmission factor in planar coordinates during first pool trace experiment (s)
$F_\mathrm{pl,Ex2}$	thermal transmission factor in planar coordinates during second pool trace experiment (s)
F_planar	thermal transmission factor in planar coordinates (unitless)
F_T	total thermal transmission factor for multisegment conduit system (unitless)
h	conduit height (m)
h_conv	water convection heat transfer coefficient ($\mathrm{W\,m^{-2}\,^\circ C^{-1}}$)
h_rad	radiation heat transfer coefficient ($\mathrm{W\,m^{-2}\,^\circ C^{-1}}$)
$H_i^{(1)}$	Hankel functions of the first kind
k_r	thermal conductivity of rock ($\mathrm{W\,m^{-1}\,^\circ C^{-1}}$)
k_w	thermal conductivity of water ($\mathrm{W\,m^{-1}\,^\circ C^{-1}}$)
L	conduit length (m)
L_e	effective conduit length (m)
L_i	length of conduit segment i (m)
Nu	Nusselt Number (unitless)

Table 6. Continued.

P_{d}	conduit dry perimeter (m)
P_{w}	conduit wetted perimeter (m)
~~Continued.~~ ~~Pe~~Pr	~~longitudinal dispersion Peclet Number (unitless)~~~~Pr~~Prandtl Number (unitless)
r	radial distance from the conduit center into the surrounding rock (m)
R	conduit radius (m)
$\mathcal{R}_{\mathrm{A}}$	recharge amplitude (°C)
$\mathcal{R}_{\mathrm{D}}$	recharge duration (s)
$\mathcal{R}_{\mathrm{D,Ex1}}$	recharge duration during first pool trace experiment (s)
$\mathcal{R}_{\mathrm{D,Ex2}}$	recharge duration during second pool trace experiment (s)
~~Re~~Re	Reynolds Number (unitless)
$\mathrm{sine}_{\mathrm{H}}$	half period of a sine function between two consective zeros (unitless)
$\mathrm{sine}_{\mathrm{O}}$	one period of a sine function from one trough to the next (unitless)
t	time (s)
t_{ft}	fluid flow-through time through the conduit, L/V (s)
$t_{\mathrm{ft},i}$	fluid flow-through time through segment i, L_i/V_i (s)
$t_{\mathrm{peak,in}}$	temperature peak at conduit beginning ($x = 0$) (°C)
$t_{\mathrm{peak,out}}$	temperature peak at conduit end ($x = L$) (°C)
T_{r}	rock temperature (°C)
$T_{\mathrm{r,0}}$	initial rock temperature (°C)
$T_{\mathrm{r},\infty}$	rock temperature at an infinite distance from conduit axis (°C)
$T_{\mathrm{r,d}}$	dry rock temperature (°C)
$T_{\mathrm{r,w}}$	wet rock temperature (°C)
T'_{r}	$T_{\mathrm{r}} - T_{\mathrm{r},\infty}$ (°C)
T_{s}	conduit surface temperature (°C)
$T_{\mathrm{s,d}}$	dry conduit surface temperature (°C or K)
$T_{\mathrm{s,w}}$	wet conduit surface temperature (°C)
T_{w}	water temperature (°C or K)
$T_{\mathrm{w,in}}$	water temperature at conduit beginning ($x = 0$) (°C)
$T'_{\mathrm{w,in}}$	$T_{\mathrm{w,in}} - T_{\mathrm{r},\infty}$ (°C)
$T_{\mathrm{w,out}}$	water temperature at conduit end ($x = L$) (°C)
~~$T'_{\mathrm{w,out}}$~~~~$T_{\mathrm{w,out}} - T_{\mathrm{r},\infty}$ (°C)~~height	

Table 6. Continued.

$T'_{\mathrm{w,out}}$	$T_{\mathrm{w,out}} - T_{\mathrm{r},\infty}$ (°C)
$T_{\mathrm{w,peak,in}}$	peak/trough water temperature at conduit beginning ($x = 0$) (°C)
$T_{\mathrm{w,peak,out}}$	peak/trough water temperature at conduit end ($x = L$) (°C)
V	flow velocity in conduit ($\mathrm{m\,s^{-1}}$)
V_0	initial flow velocity in conduit ($\mathrm{m\,s^{-1}}$)
V_{A}	flow velocity amplitude ($\mathrm{m\,s^{-1}}$)
V_{e}	equivalent flow velocity in conduit ($\mathrm{m\,s^{-1}}$)
V_i	flow velocity in conduit of segment i ($\mathrm{m\,s^{-1}}$)
$\overline{V}$	average or reference flow velocity ($\mathrm{m\,s^{-1}}$)
W_{fs}	width of the water free surface (m)
x	longitudinal position along conduit (m)
y	distance from the conduit center into the surrounding rock (m)
α_{r}	thermal diffusivity of rock ($\mathrm{m^2\,s^{-1}}$)
ϵ	roughness height (m)
Θ	~~advection and conduction~~ conduction and advection time ratio (unitless)
$\lambda_{\mathrm{T,sin}}$	thermal length scale for sinusoidal temperature variations (m)
$\Lambda_{\mathrm{T,sin}}$	thermal process number (unitless)
μ_{w}	dynamic viscosity of water ($\mathrm{kg\,m^{-1}\,s^{-1}}$)
ρ_{r}	density of rock ($\mathrm{kg\,m^{-3}}$)
ρ_{w}	density of water ($\mathrm{kg\,m^{-3}}$)
σ	width of thermal Gaussian pulse (s)
σ_{SB}	Stefan-Boltzmann constant ($\mathrm{W\,m^{-2}\,K^{-4}}$)
τ	retardation of thermal peak/trough (s)
$\cancel{\tau_{\mathrm{Ex1}}}\tau_i$	retardation of thermal peak~~during first pool trace experiment~~ /trough for segment i (s)
$\cancel{\tau_{\mathrm{Ex2}}}\tau_{\mathrm{pl,Ex1}}$	retardation of thermal peak ~~during second~~ in planar coordinates during first pool trace experimen
$\cancel{\tau_i}\tau_{\mathrm{pl,Ex2}}$	retardation of thermal peak ~~/trough for segment i~~ in planar coordinates during second pool trace
τ_{planar}	retardation of thermal peak/trough in planar coordinates (s)
τ_{T}	total retardation of thermal peak/trough for multisegment conduit system (s)
Ψ	$\rho_{\mathrm{w}} c_{p,\mathrm{w}} / (\rho_{\mathrm{r}} c_{\mathrm{p,r}})$ (unitless)
ω	angular frequency

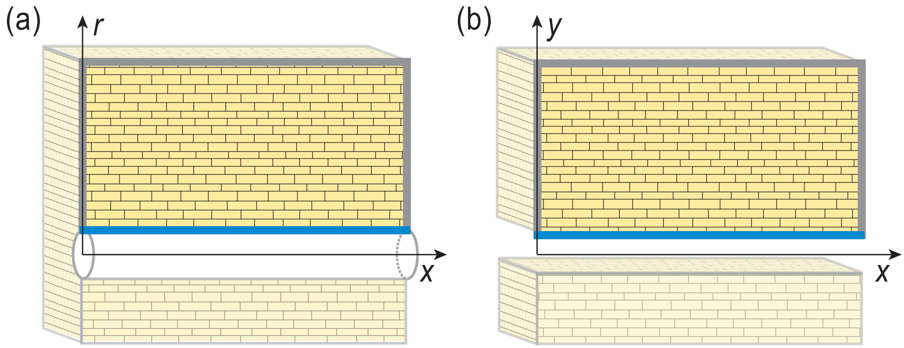

Figure 1. Model setup for heat transport simulations involving a **(a)** conduit or **(b)** fracture and the surrounding rock. The advection-dispersion equation is solved along the 1-D **(a)** conduit or **(b)** fracture. Because of symmetry, conduction in the 3-D rock surrounding the conduit or fracture may be modeled with a simple 2-D rectangle (outlined in thick gray and blue lines). Thus, conduction is modeled in **(a)** 2-D cylindrical or **(b)** 2-D planar coordinates. The two geometries are coupled to each other at each respective thick blue line (i.e., the conduit/fracture wall surface). Thick gray limestone boundaries perpendicular to the conduit or fracture are insulated rock boundaries. Thick gray limestone boundaries parallel to the conduit or fracture are sufficiently far from flow path lines to satisfy Eqs. (7) or (9), respectively, and are set to background temperature.

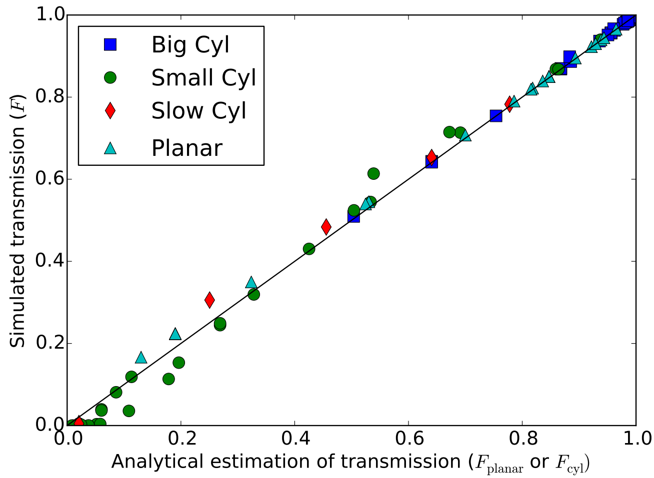

Figure 2. A comparison of the transmission factors of peaks in the simulations of Gaussian temperature pulses against the modified form of the analytical solution for a sinusoidal input temperature (Eq. 36). Cylindrical cases are corrected by an additional factor (Eq. 37) that is a function of the dimensionless parameter Θ. These modified forms of the analytical solution provide a close fit to the simulation results for most cases. Big Cyl and Small Cyl indicate a conduit in cylindrical coordinates with a $D_{\mathrm{H}} \geq 1\,\mathrm{m}$ and a $D_{\mathrm{H}} < 1\,\mathrm{m}$, respectively. Slow Cyl indicates a conduit in cylindrical coordinates with a $V \leq 0.0352\,\mathrm{m\,s^{-1}}$. Planar indicates a conduit in planar coordinates.

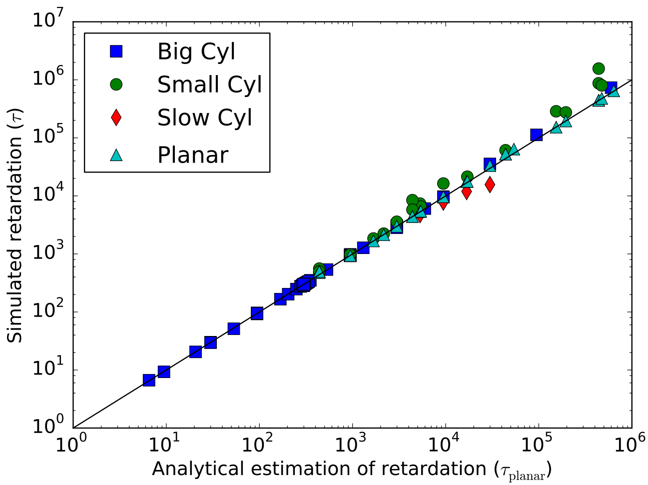

Figure 3. Simulated retardation as a function of theoretical retardation. In general, there is excellent agreement between the analytical solution and numerical simulations. Legend categories are the same as Fig. 2.

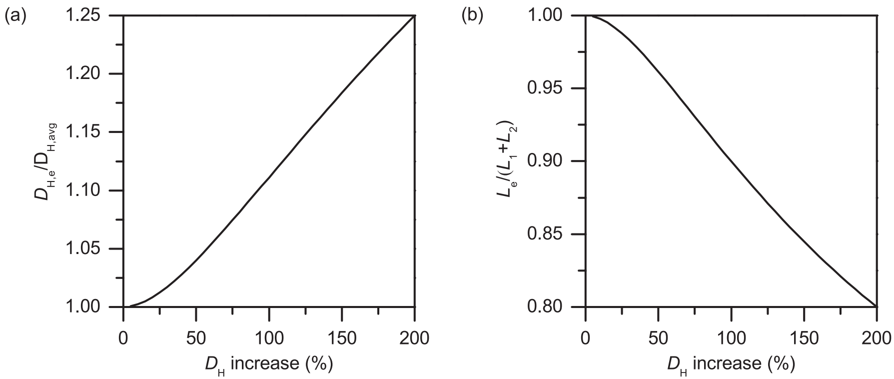

Figure 4. (a) $D_{\mathrm{H,e}}/D_{\mathrm{H,avg}}$ and **(b)** $L_\mathrm{e}/(L_1+L_2)$ for different relative increases in D_H when $L_1 = L_2$. The $D_{\mathrm{H,e}}$ for a flow path with two sections of different D_H is generally more heavily weighted toward the section with a larger D_H, and a larger increase in D_H produces a larger $D_{\mathrm{H,e}}$. The L_e for a flow path with two sections of different D_H is always less than $L_1 + L_2$, and a larger increase in D_H results in a smaller L_e.

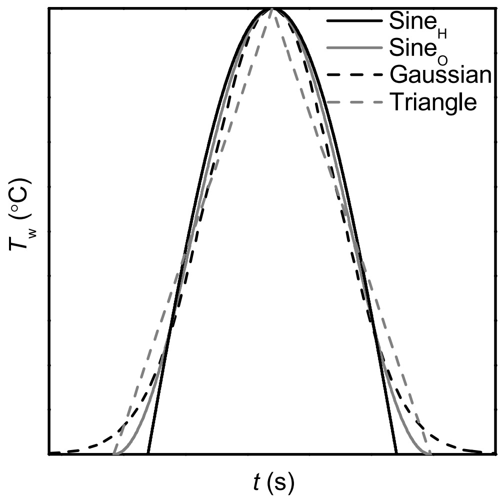

Figure 5. Different modeled recharge shapes. The sine$_H$ curve is widest near the peak and produces less damping and more retardation than the other recharge shapes. Note the ends of the Gaussian curve are not shown in this figure.

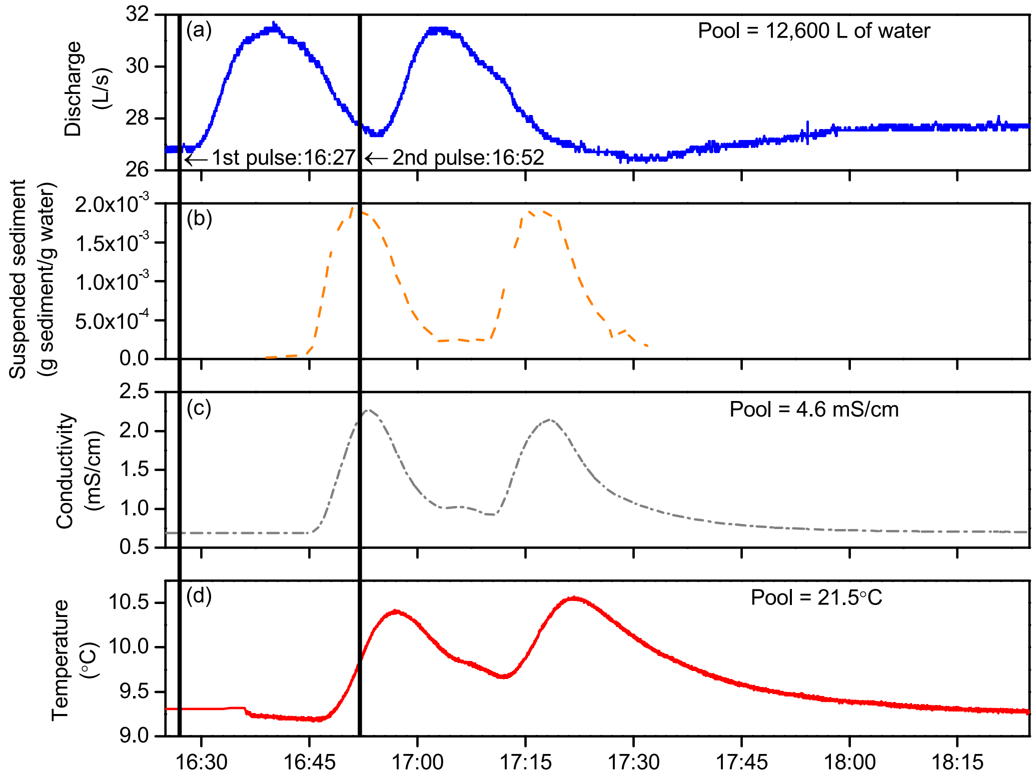

Figure 6. (a) Discharge, **(b)** suspended sediment, **(c)** electrical conductivity, and **(d)** temperature breakthrough curves at Freiheit Spring on 2 September 2010. Water was added to a pool at the edge of a sinkhole, and the water was heated to 21.5°C as salt was added. The water was emptied into the sinkhole, and breakthrough curves were monitored at Freiheit Spring approximately 95 m away.